LMSC-HREC TR D497400

Lockheed

Missiles & Space Company, Inc.

HUNTSVILLE RESEARCH & ENGINEERING CENTER

Cummings Research Park
4800 Bradford Drive,
Huntsville, Alabama

ANALYTICAL SUPPORT FOR SPAR EXPERIMENT 76-36

FINAL REPORT

Prepared under Contract No. NAS8-32401

Investigators

Sidney V. Bourgeois
Philomena G. Grodzka
John E. Pond
Lawrence W. Spradley

LOCKHEED MISSILES & SPACE COMPANY, Inc.
Huntsville Research & Engineering Center
Huntsville, AL 35807

For

NASA-GEORGE C. MARSHALL SPACE FLIGHT CENTER
Huntsville, Alabama

APPROVED: George D. Remy
for J.S. Farrior
Resident Director

August 1977

ABSTRACT

Thermal, convection, and rotational fluid flow analyses were conducted of a prototype of the SPAR experiment 76-36. A constitutional supercooling criterion (CSC) was calculated from the thermal data. The study results include the following:

- Cooling rates have been identified for generating thermal conditions such that freezing occurs within the allocated low-g time; thermal and solutal convection velocities are of the order of 10^{-3} cm/sec at 10^{-4}g; and the CSCs are approximately those of the SPAR experiment 74-21.
- An experiment orientation with respect to the rocket spin axis has been identified which should ensure optimum damping times of rotational motion.

FOREWORD AND ACKNOWLEDGMENTS

This document reports the results of a five-month study conducted by personnel of the Lockheed-Huntsville Research & Engineering Center under Contract NAS8-32401 and entitled "Analytical Support for SPAR Experiment 76-36" for NASA-Marshall Space Flight Center. The stated contract requirements are:

I. Objectives

The objectives of this study are:

A. Provide analytical support for fluid flow phenomena in SPAR Experiment 76-36.

B. Provide comparison analyses between SPAR Experiments 74-21 and 76-36 for the purpose of experiment design.

II. Statement of Work

The contractor shall provide the necessary personnel and facilities to perform the following tasks:

Task I: The contractor shall map the thermal profile in the melt for each of the three alloy systems in SPAR Experiment 76-36.

Task II: The contractor shall map anticipated fluid flow due to solutal and buoyancy driven convection in the sample materials during the Sounding Rocket Flight.

Task III: The contractor shall compare the low-gravity fluid flow obtained in SPAR Experiment 74-21 with that expected in SPAR Experiment 76-36. Design criteria for sizing the alloy samples will be provided so that the two SPAR Experiments will have identical initial fluid flow and thermal fields.

The NASA contract monitors for this investigation were Dr. M. H. Johnston and Ms. C. S. Griner of MSFC/M&P.

The authors thank Dr. L. L. Lacy of MSFC/SSL for making available his data on spin-down times and Dr. G. Fichtl, also of MSFC/SSL, for the stimulating discussion of spin generated fluid flows and damping times.

CONTENTS

INTRODUCTION

One of the first studies of dendrite crystal growth in low-g environments was the series of experiments performed in the period 1975-77 on Black Brandt VC sounding rocket flights (SPAR Experiment 74-21). In these early experiments, dendrite crystals of ammonium chloride were grown from aqueous solutions cooled below supersaturation. The low-g crystallizations were recorded on film and subsequently compared with crystals crystallized on the ground. The low-g crystallization showed a number of different behaviors from those observed in the 1-g cases (Ref. 1).

Two aspects of the ammonium chloride crystallizations in low-g are of interest. The basic phenomenon of dendritic crystallization in the absence of convection is of intrinsic importance. Of particular interest is the origin of the secondary nucleation of detached crystals occuring after the primary dendrite stalks have been nucleated and grown awhile. Some theories hold that convection breaks off delicate dendrite arms and sweeps them into the bulk of the melt. Other theories hold that the nucleation arises from an interplay of thermal and constitutional conditions. In a more applied vein, the crystallization of ammonium chloride can serve as a useful model for metal alloy crystallization both in 1-g and low-g. In order to be a useful model for metal alloy crystallization, however, convective fluid flow (velocities and flow patterns) and constitutional supercooling conditions need to be made similar.

As discussed in a prior report (Ref. 2), making similar both convective and constitutional supercooling conditions for the case of 1-g gravity would involve a more lenghty study than can be undertaken at this time. In low-g conditions, however, convective velocities can be reduced to insignificant levels ($\sim 10^{-4}$ or 10^{-5} cm/sec). The only concern thus becomes that of similarizing constitutional supercooling conditions. Accordingly one of the

objectives of a second series of rocket experiments of dendrite growth is to freeze molten metal systems in low-g under themal conditions such that the constitutional supercooling conditions are generally the same as for the first ammonium chloride low-g crystallizations (SPAR Experiment 74-21). The data from the 74-21 and 76-36 should then show that ammonium chloride crystallizations can be a useful model for metal alloy crystallization as well as providing basic data on dendrite crystallization in general.

The purpose of the present study is to provide preliminary thermal and convective analysis data for the 76-36 experiment in order to ensure that the experimental furnace will provide the desired constitutional supercooling and convective conditions. The approach used consists of four parts:

- Thermal analysis of a preliminary furnace design to ensure that the metal samples are completely frozen in the available low-g time period (about 5 to 7 min) of the SPAR rocket test, to provide data for determining the supercooling parameter, and to provide thermal boundary conditions for the convection analyses.
- Calculations of a supercooling criterion (G/RA ratio, where G is the temperature gradient at the crystallizing interface, R is the crystal growth rate, and A is a constant for a given solute concentration), for the various cases.
- A convection analysis of the various cases to ensure that convective velocities will not exceed about 10^{-2} cm/sec in the low-g tests.
- An analysis of damping times for fluid flow generated by rocket spin-up and spin-down.

Each of these areas is discussed in detail in following sections as is a description of the general nature of the apparatus, materials, and procedures.

EXPERIMENT DESCRIPTION, APPARATUS, AND MATERIALS

The SPAR 76-36 Experiment entitled "Comparative Alloy Solidification" will consist of melting a metal alloy sample on the ground and bringing it up to some designated constant temperature (soak temperature) just prior to the rocket flight. During launch and about 2 min after the rocket enters the low-g period, the soak temperature will be maintained. Cooling at the sides of the cell will commence after the 2 min damping period. Solidification during the test will be somewhat as shown in the following two-dimensional representation.

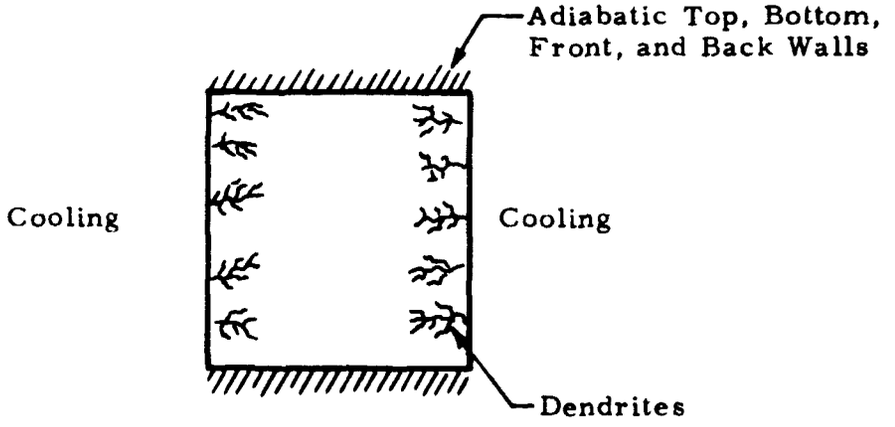

Fig. 1 - Two-Dimensional Schematic of Experiment 76-36 Crystallization

The sample will be completely frozen by the time the low-g period is completed and the rocket starts its descent to earth. The frozen samples will be retrieved and analyzed on earth by various metallographic techniques.

A prototype furnace design to accomplish the required solidifications is shown in Fig. 2.

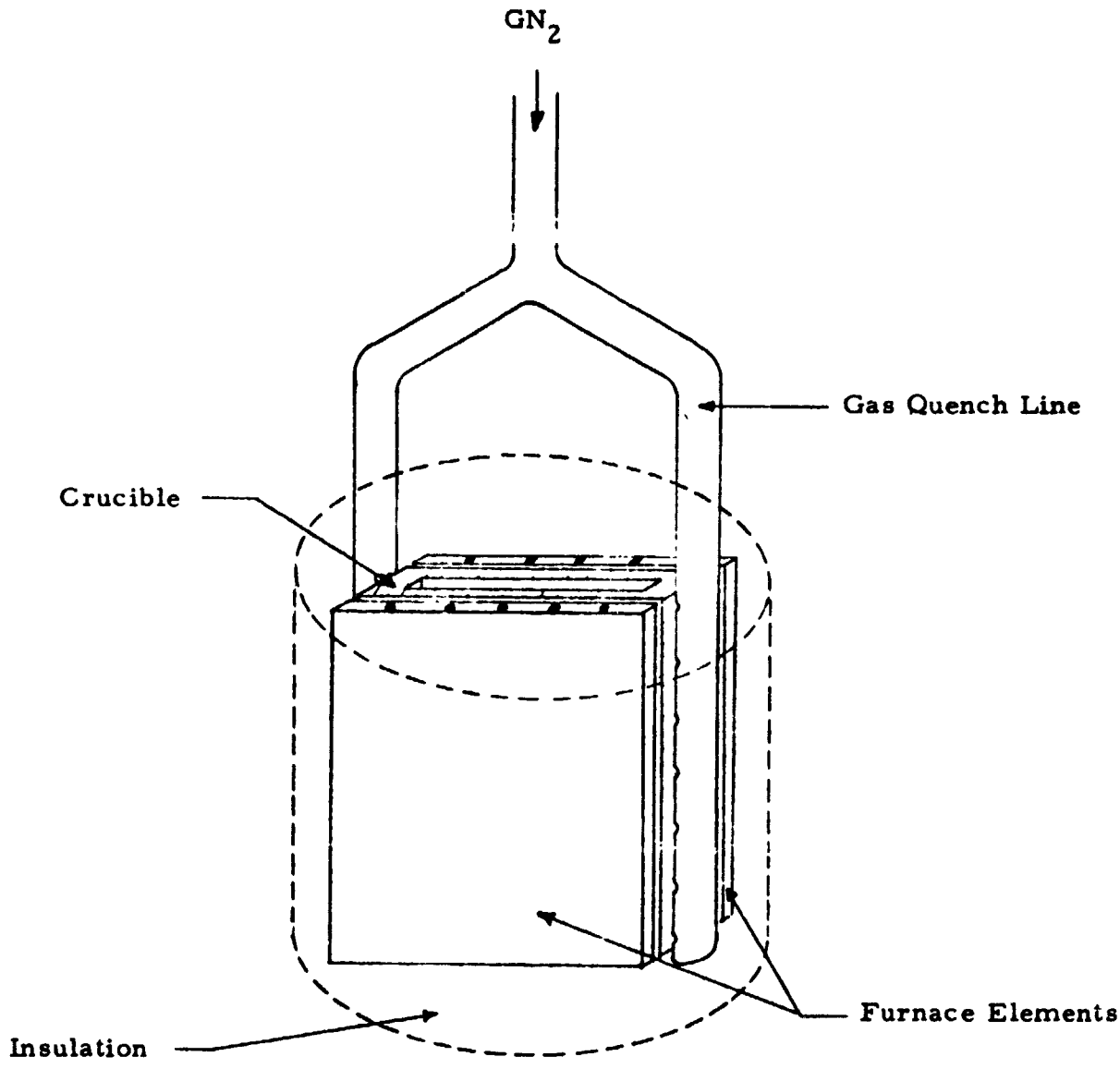

Fig. 2 - Protoflight Furnace

The crucible will be constructed of graphite and will have the dimensions (first-cut) shown in Fig. 3.

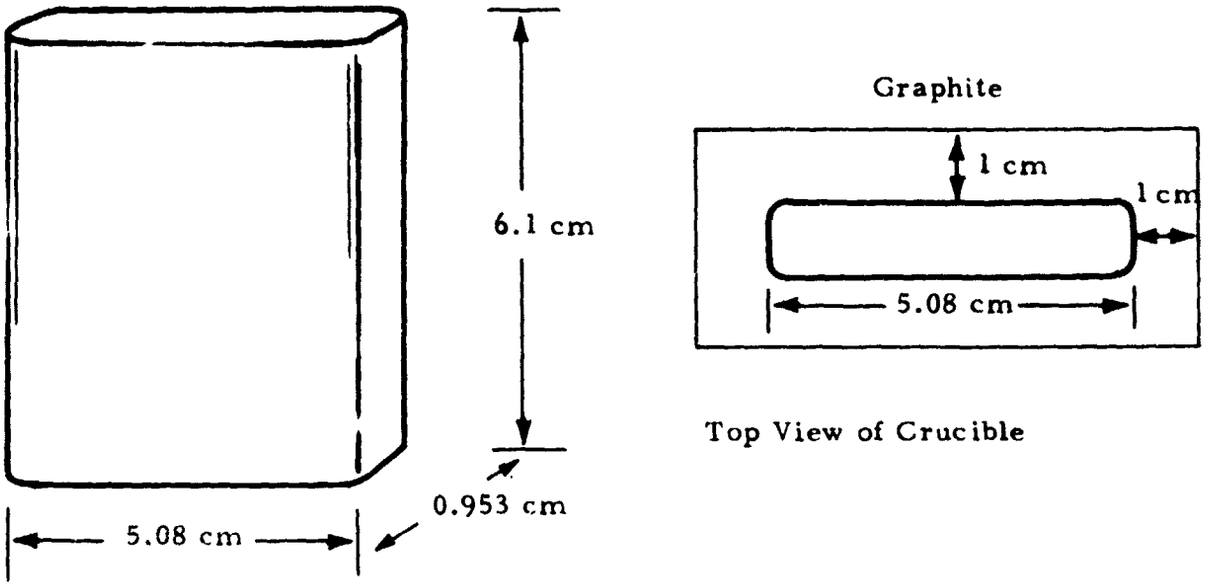

Fig. 3 - Dimensions of Graphite Crucible

The metal alloy systems to be used in the tests are given in Table 1.

Table 1

EXPERIMENTAL METAL ALLOY SYSTEMS

Metal Melt	Dendrites Enriched by	Melt Enriched by	Generated Buoyancy Direction
Sn – 50 wt% Pb	Pb	Sn	↑
Aℓ – 4.5 wt% Cu	Aℓ	Cu	↓
Sn – 3 wt% Bi	Sn	Bi	↓

Liquid and solid physical property data for the metal alloy systems as well as for the aqueous ammonium chloride solution of Experiment 74-21 are given in Tables 2 and 3.

The following symbol identification is used in the tables.

ρ = density
c = heat capacity
λ = heat of fusion
k' = thermal conductivity
μ = viscosity
β_T = thermal expansivity
β_c = solutal expansivity
ν = kinematic viscosity
α = thermal diffusivity
D = solutal diffusivity

Table 2

LIQUID PHYSICAL PROPERTIES IN CGS UNITS*

	Sn-50 P_b	Al-4.5 Cu	Sn-3 Bi	H_2O-27.8
T_m	211	644	283	26
ρ	7.81	2.46	7.06	1.08
C	0.046	0.240	0.059	0.740
k'	0.055	0.220	0.076	0.0012
μ	0.0133	0.0149	0.0184	0.01
β_T (1/K)	$1.07\ 10^{-4}$	$1.12\ 10^{-4}$	$1.01\ 10^{-4}$	$2.95\ 10^{-4}$
β_C (1/w+%)	$-3.0\ 10^{-3}$	–	–	$-2.81\ 10^{-3}$
D	$3.0\ 10^{-5}$	–	–	$1.8\ 10^{-5}$
ν	$1.7\ 10^{-3}$	$6.1\ 10^{-3}$	$2.6\ 10^{-3}$	$9.3\ 10^{-3}$
α	0.15	0.37	0.18	$1.5\ 10^{-3}$
Pr ($=\nu/\alpha$)	0.011	0.016	0.014	6.2
$\beta_T/\nu\alpha$	0.42	0.05	0.22	21.2
β_T/ν^2	37.0	3.0	14.9	3.4

*cm, gm, sec, C, cal, poise, etc.

Table 3

SOLID PHYSICAL PROPERTIES IN CGS UNITS*

	Sn-50 Pb	Al-4.5 Cu	Sn-3 Bi	Graphite
ρ	8.32	2.81	5.84	2.25
C	0.05	0.23	0.06	0.17
λ	12.8	93.0	14.5	–
k'	0.12	0.33	0.08	0.06

*cm, gm, sec, C, cal, poise, etc.

THERMAL ANALYSES

Temperature profiles as a function of time within the cell at various conditions of cooldown were computer calculated. The Lockheed Thermal Analyzer Program was utilized. This program is applicable for cases of heat conduction within a body. Convection on the boundaries is handled by means of a heat transfer coefficient. The latent heat generated during solidification is handled in the program by ordering the program to decrease the heat capacity (sufficient to allow liberation of the latent heat) at a node when the temperature reaches the freezing point. Such a procedure is fairly standard for computer calculations involving phase change. The cell was modeled according to the schematic shown in Fig. 4.

Order of magnitude cooling rates were determined from a simple calculation of cooling rate required to freeze each melt within 360 sec. The formula used for this calculation is given by Eq. (1).

$$Q \cong \frac{k\Delta T}{2} \frac{\pi}{\alpha t} \qquad (1)$$

where

k = thermal conductivity
$\Delta T = T_{initial} - T_{freeze}$
t = 360 sec
Q = cooling rate
α = thermal diffusivity

The results of applying this equation to each of the melts are shown below.

Melt	Q (cal/cm^2-sec)	ΔT (C)
Sn - 50 Pb	0.50	90
Al - 4.5 Cu	2.86	155
Sn - 3 Bi	0.50	113

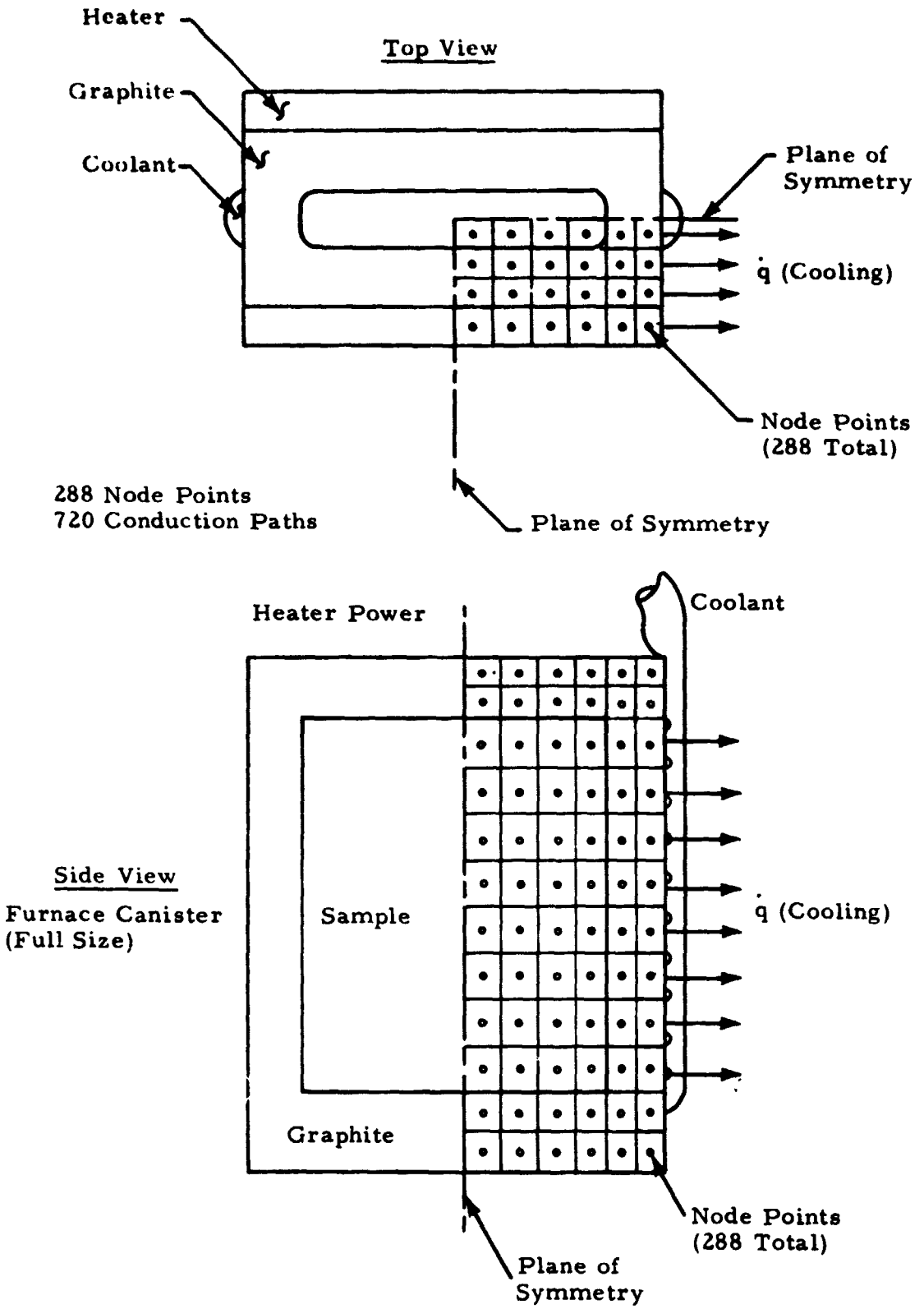

Fig. 4 - Computer Model of 76-36 Experiment

Using a value near the above estimate for Q, the Sn-50 Pb system temperature profiles are shown in Fig. 5. The model currently assumes that the ceramic heaters behave thermally like graphite and that all surfaces are adiabatic except those cooled by the gas.

A number of cases were run varying soak temperature and cooling rates to provide data for calculation of the supercooling criterion, as discussed in the next section, and to provide boundary conditions for the convection analysis discussed in a following section.

Isotherm profiles (Figs. 6 through 9) calculated by the Thermal Analyzer Program revealed a potentially significant furnace design factor. This factor consists of the sharply curved isotherms (isotherm profiles shown as views from the top looking down — "horizontal cuts"). The intent of the experiment is to freeze the metal with flat isotherms. These isotherms will be parallel to the cooling walls. Thus the final furnace design should take these curved isotherms into account, and design alternatives should be explored which will minimize these undesirable effects.

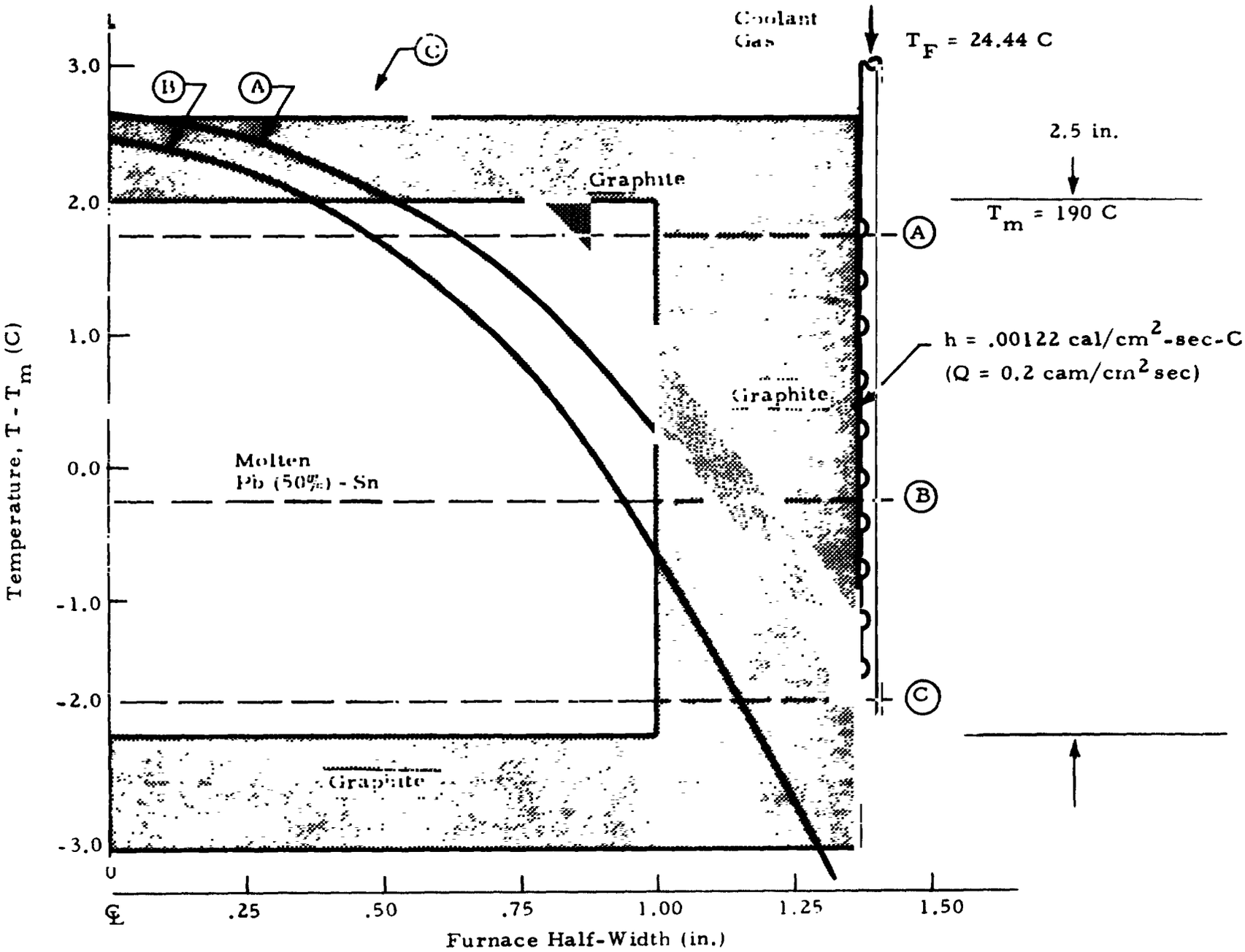

Fig. 5 - SPAR 76-36 Temperature Profiles 150 sec After Cooling from a 210 C Soak

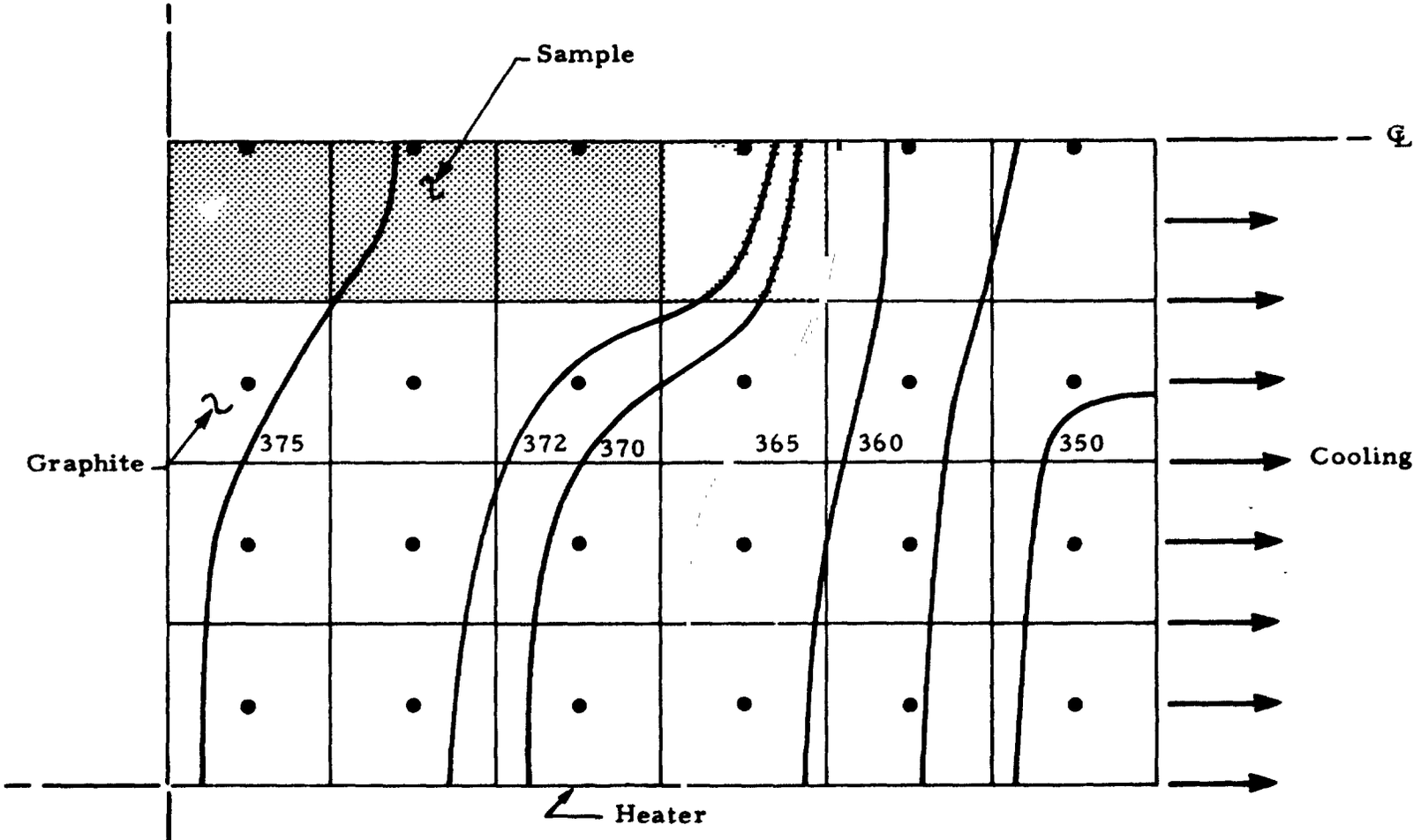

Fig. 6 - Furnace Isotherm Profiles for Sn Pb (Case 23, 50 sec After Quench Begins, Values in Degrees Fahrenheit; Soak Temperature, 401 F (205 C))

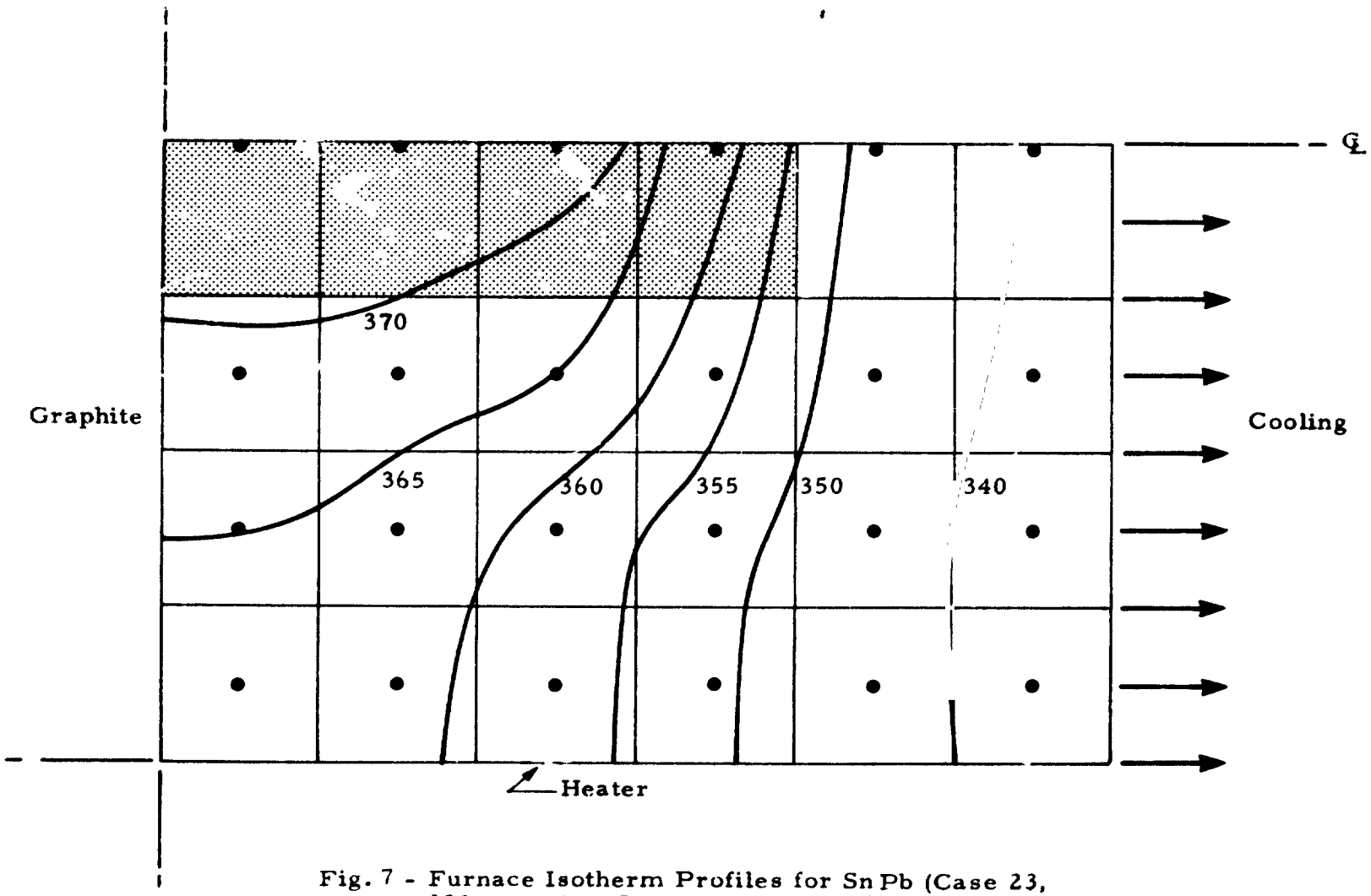

Fig. 7 - Furnace Isotherm Profiles for Sn Pb (Case 23, 120 sec After Quench Begins, Values in Degrees Fahrenheit; Soak Temperature, 401 F (205 C))

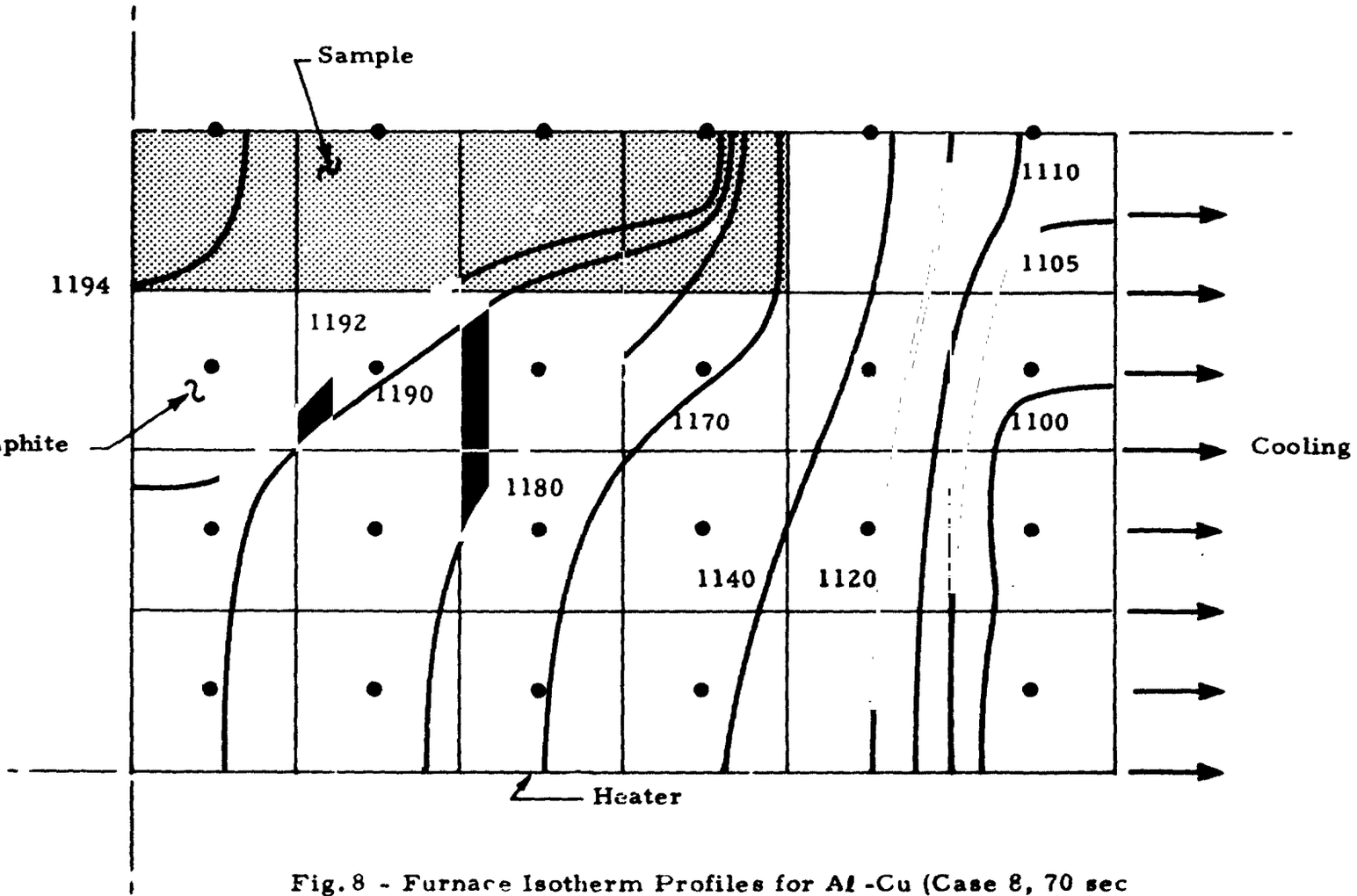

Fig. 8 - Furnace Isotherm Profiles for Al-Cu (Case 8, 70 sec After Quench Begins, Values in Degrees Fahrenheit; Soak Temperature, 1346 F (730 C))

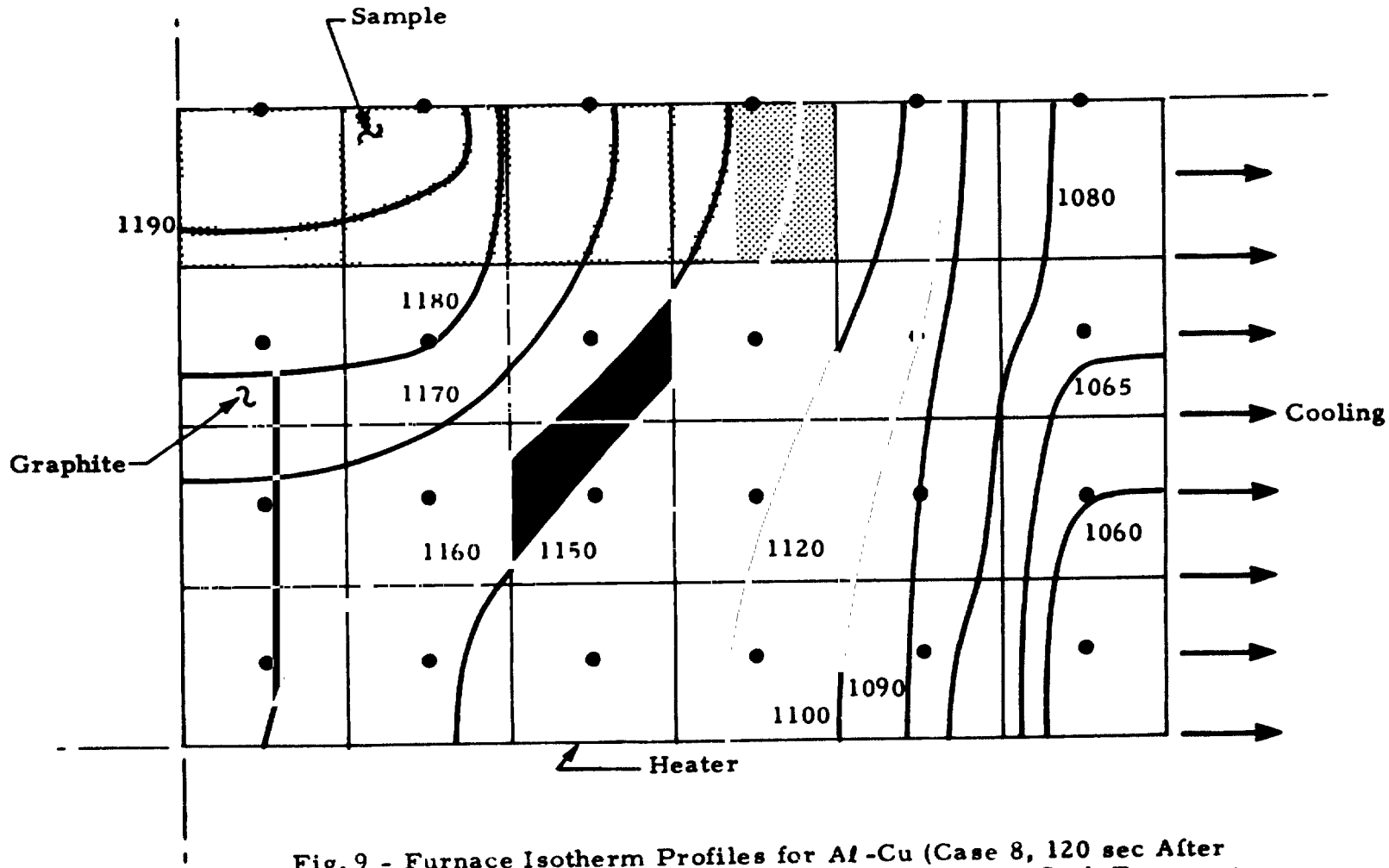

Fig. 9 - Furnace Isotherm Profiles for Al-Cu (Case 8, 120 sec After Quench Begins, Values in Degrees Fahrenheit; Soak Temperature, 1346 F (730 C))

CONSTITUTIONAL SUPERCOOLING CRITERION (CSC)

The liquidus temperature gradient $(\partial T_L/\partial x')_{x'=0}$ ahead of a solidifying interface can be shown to be given by the following equation (Ref. 3 gives a simple derivation).

$$(\partial T_L/\partial x')_{x'=0} = - m R C^o (1 - k)/kD$$

where

T_L = liquidus temperature
C^o = initial solute concentration
m = slope of the liquidus curve
k = segregation coefficient
D = solute diffusivity
R = rate of freezing
x' = location of the moving solid/liquid interface

If the actual temperature gradient at the interface is G, we can specify a constitutional supercooling parameter (CSC) as follows:

$$CSC = \frac{G}{(\partial T/\partial x')_{x'=0}} = - \frac{G}{m R C^o (1 - k)/k D} = \frac{G}{RA}$$

The CSC parameter can thus be viewed as a dimensionless supercooling parameter. If CSC is less than one then the liquidus temperature gradient is steeper than the actual temperature gradient and constitutional supercooling prevails. A value greater than one has the opposite meaning — the liquid melt is constitutionally superheated.

Although it would seem that the CSC parameter — giving as it does the relative degree of supercooling — should also be an excellent indicator of

crystal morphology, no one has yet thought to test such a relationship. A number of prior studies have tried to correlate G/R or $G/R^{1/2}$ with crystal morphology (Refs. 4, 5 and 6) and have achieved varying success. One possible complication not considered thus far is that relatively slow crystal growth kinetics can result in considerable thermal as well as constitutional undercooling. A test of the correlation of the CSC parameter with crystal morphology is a study planned for the future by the present investigators. Tables 4 through 6 show the value of the CSC parameter for various cases. As indicated in the tables, the CSC value at the time of initial freezing for the NH_4Cl in Experiment 74-21 was approximately 0.01. Thus, the results for all three metal systems of Experiment 76-36 are of the same order of magnitude as occurred in Experiment 74-21. Thus, the metal-model results of Experiment 74-21 should be especially appropriate to those of Experiment 76-36. A more detailed account of the CSC throughout the whole period of freezing, however, is indicated in any future analysis.

Table 4

CALCULATED THERMAL RESULTS FOR Sn-50 Pb

Case	T_{soak} (C)	$Q\left(\frac{cal}{cm^2\text{-sec}}\right)$	t_I (sec)	t_F (sec)	$G\left(\frac{C}{cm}\right)$	$R\left(\frac{cm}{sec}\right)$	$\frac{G/R^*}{A}$
19	275	1.0	180	–	3.149	.003030	0.003
20	275	2.0	100	210	2.85	.01505	0.001
21	275	5.0	40	120	12.99	.01859	0.002
22	205	0.5	50	260	1.762	.00436	0.001
23	205	0.7	40	200	1.447	.00796	0.001
24	205	1.0	30	160	1.706	.011569	0.001

*G/R taken at time of initial freezing; A = $3.95 \cdot 10^5$ C-sec/cm^2 for Sn Pb; $\frac{G/R}{A}$ = 0.01 for $NH_4C\ell$ in Experiment 74-21.

Table 5

CALCULATED THERMAL RESULTS FOR Aℓ-4.5 Cu

Case	T_{soak} (C)	Q $\left(\frac{cal}{cm^2\text{-sec}}\right)$	t_l (sec)	t_F (sec)	G $(\frac{C}{cm})$	R $(\frac{cm}{sec})$	$\frac{G/R^*}{A}$
7	730	1.0	170	370	1.058	.00644	0.006
8	730	3.0	60	150	3.250	.01788	0.006
9	730	5.0	40	100	3.963	.0309	0.004
10	660	0.2	140	–	0.229	.00148	0.005
11	660	0.6	50	310	0.480	.00473	0.004
12	660	1.0	30	210	1.160	.00715	0.006

*G/R taken at time of initial freezing; A = 2.86 10^4 C-sec/cm^2 for Aℓ-Cu; $\frac{G/R}{A}$ = 0.01 for NH_4 Cℓ in Experiment 74-21.

Table 6

CALCULATED THERMAL RESULTS FOR Sn-3 Bi

Case	T_{soak} (C)	$Q\left(\frac{cal}{cm^2\text{-sec}}\right)$	t_i (sec)	t_F (sec)	$G\left(\frac{C}{cm}\right)$	$R\left(\frac{cm}{sec}\right)$	$\frac{G/R^*}{A}$
28	313	1.0	180	–	2.88	.00573	0.26
29	313	2.0	100	200	2.45	.0179	0.07
30	313	5.0	40	110	11.80	.0235	0.26
31	240	.5	50	260	1.07	.0059	0.09
32	240	.7	30	190	2.34	.00624	0.19
33	240	1.0	20	150	3.48	00818	0.22

*G/R taken at time of initial freezing; A = 1.95 10^3 C-sec/cm^2 for Sn Bi; $\frac{G/R}{A}$ = 0.01 for NH_4 Cℓ in Experiment 74-21.

CONVECTION ANALYSIS

A convection analysis was conducted of two-dimensional, transient thermally-driven and solutally-driven convection for each of the three metal systems at a gravity level of 10^{-4} g_e.

The container wall temperatures versus time, for each metal case studied, are shown in Figs. 10, 11 and 12. These temperatures were taken from the thermal analyses results. The Grashof and Raleigh numbers shown in these figures are "normalized," and the actual values of Gr and Ra for a given case are obtained by multiplying by $\Delta T/T_o$ (degrees Kelvin) or by $\Delta C/C_o$ (wt%) for thermal and solutal, respectively.

The thermally driven convection results are shown in Figs. 13 through 18. The results are in the form of velocity vector maps and isotherm plots at a given instant of time. For each metal, results are shown for an early time and a late time during the freezing cycle. The effects of the moving crystallization front on the flow were ignored, thus predicted flow velocities for later times will be higher than actual. Predicted trends, however, should remain valid. Maximum predicted velocities are of the order-of-magnitude 10^{-2} cm/sec.

The solutally driven convection results are shown in Figs. 19 through 24. The data are presented in the form of velocity vector and isoconcentration plots for early and late times (in the freezing cycle) for each metal system. Again, maximum predicted velocities are less than 10^{-2} cm/sec.

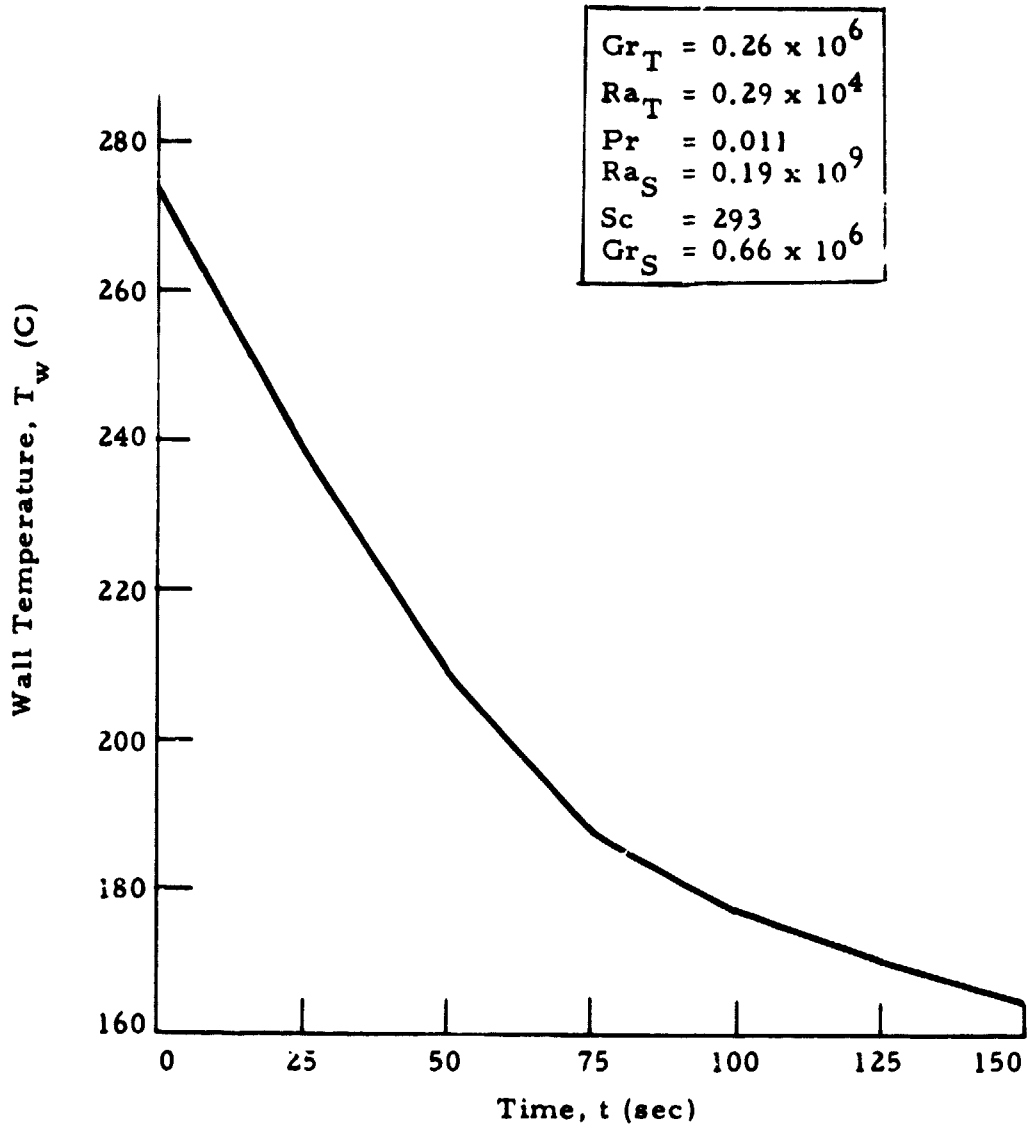

Fig. 10 - SnPb, Case 20, g = 10^{-4}, Wall Temperature vs Time

$Gr_T = 0.36 \times 10^5$
$Ra_T = 0.59 \times 10^3$
$Pr = 0.016$
$Ra_S = 0.11 \times 10^8$
$Sc = 175$
$Gr_S = 0.63 \times 10^5$

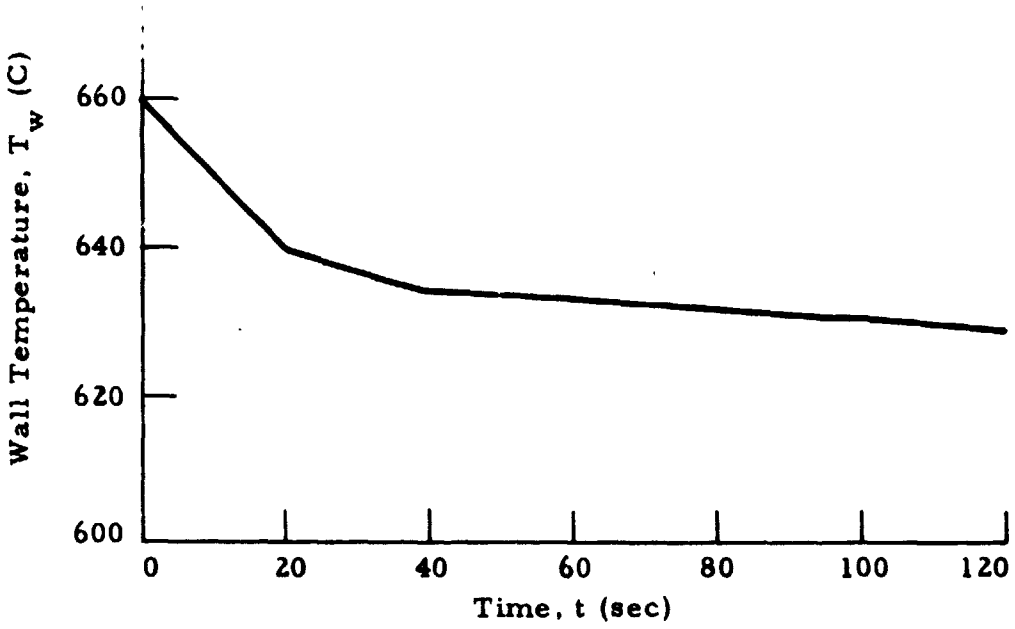

Fig. 11 - Al Cu, Case 12, $g = 10^{-4}$, Wall Temperature vs Time

$Gr_T = 0.11 \times 10^6$
$Ra_T = 0.16 \times 10^4$
$Pr = 0.014$
$Ra_S = 0.92 \times 10^6$
$Sc = 32$
$Gr_S = 0.28 \times 10^5$

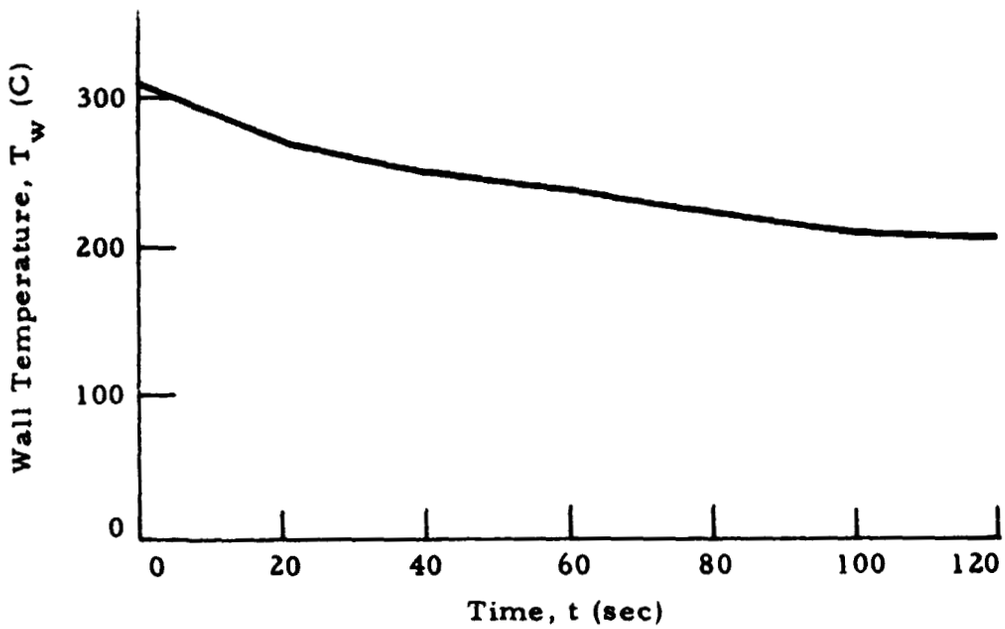

Fig. 12 - SnBi, Case 29, $g = 10^{-4}$, Wall Temperature vs Time

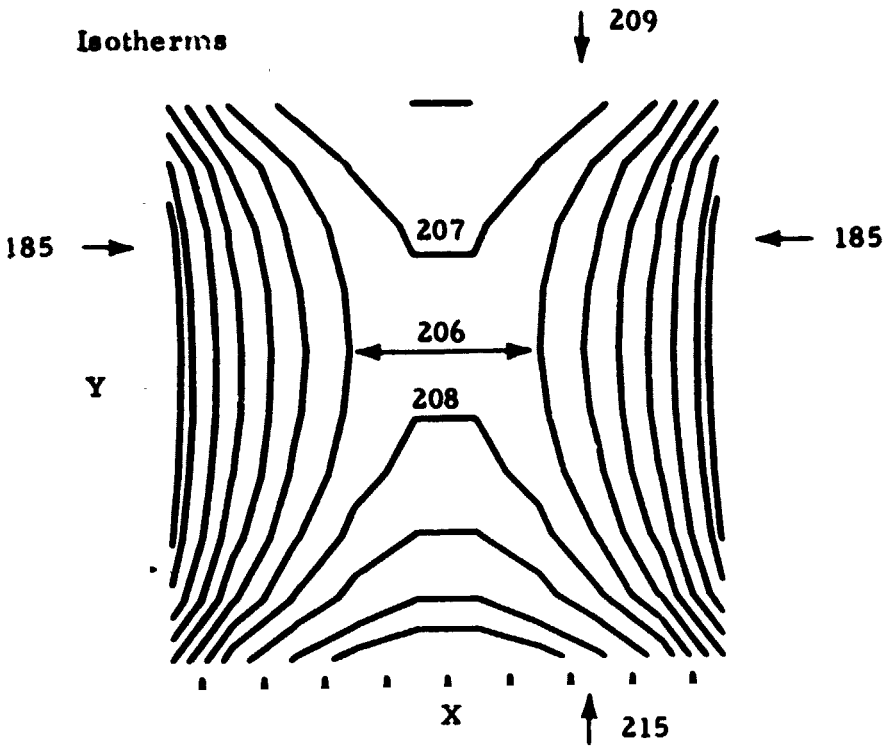

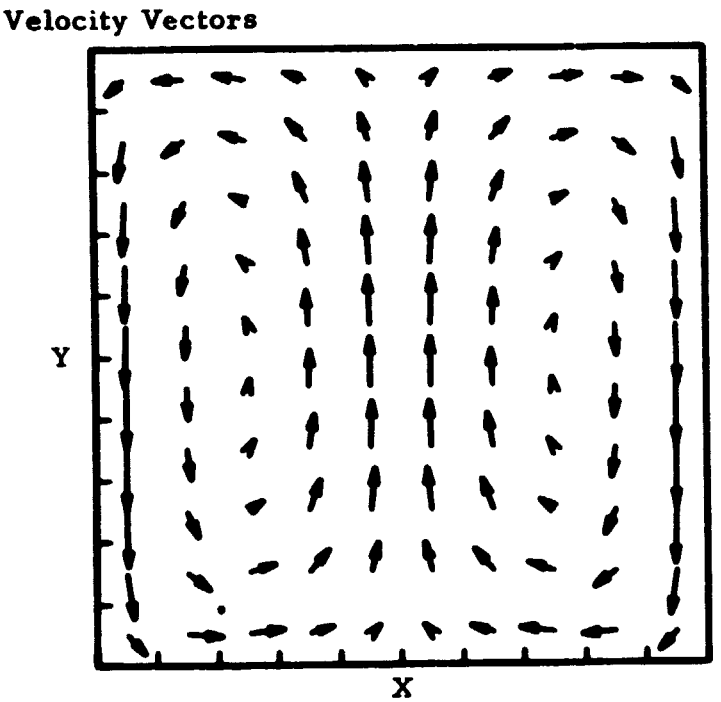

Fig. 13 - Isotherms and Velocity Profiles at t = 80 sec for SnPb Case 20 (Thermal Convection); $V_{max} = 4.7 \cdot 10^{-3}$ cm/sec; Isotherms in Degrees Celsius

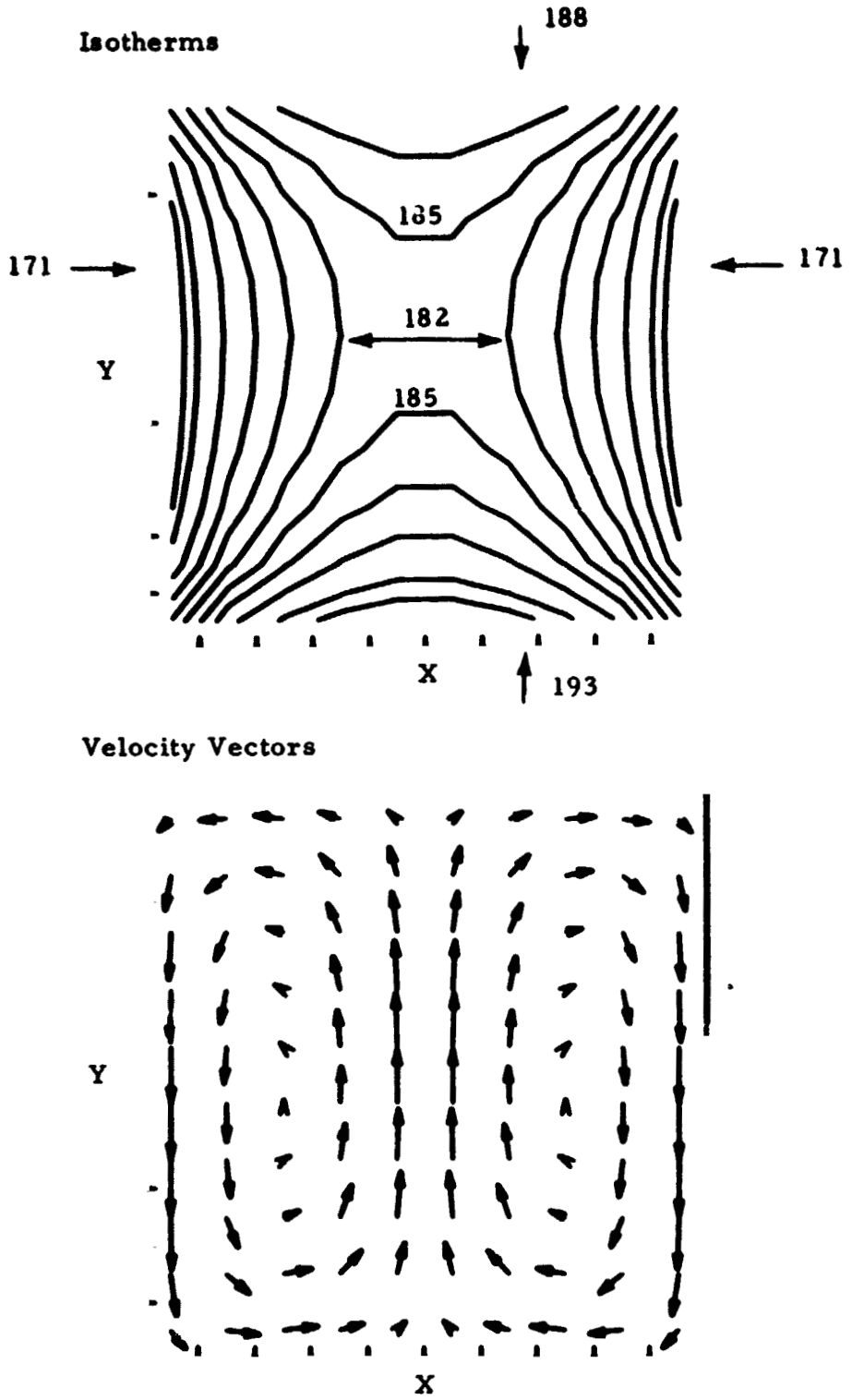

Fig. 14 - Isotherms and Velocity Profiles at t = 120 sec for SnPb Case 20 (Thermal Convection); $V_{max} = 5.2 \cdot 10^{-3}$ cm/sec; Isotherms in Degrees Celsius

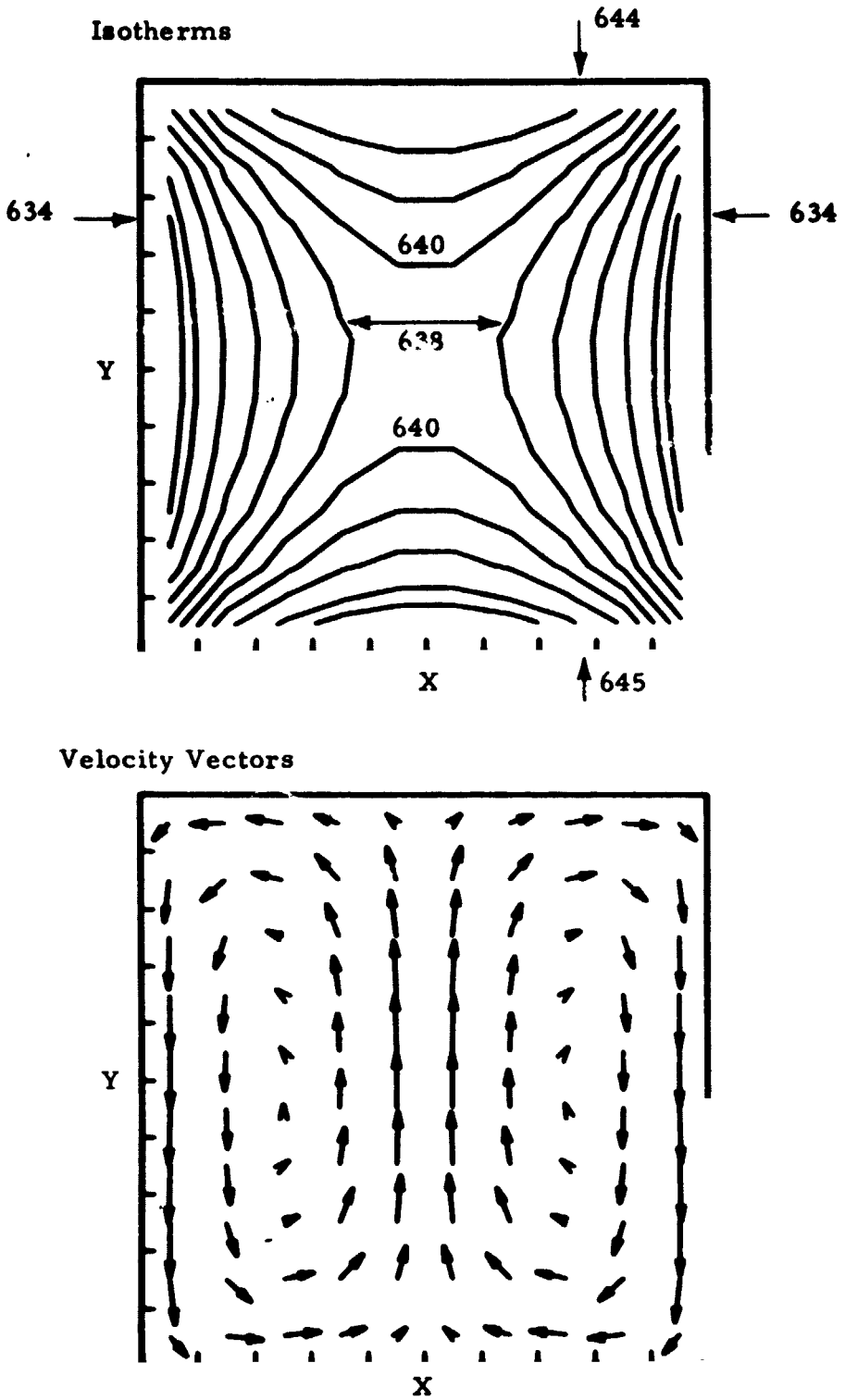

Fig. 15 - Isotherms and Velocity Profiles at t = 40 sec for Al Cu Case 12 (Thermal Convection); $V_{max} = 6.3 \cdot 10^{-4}$ cm/sec; Isotherms in Degrees Celsius

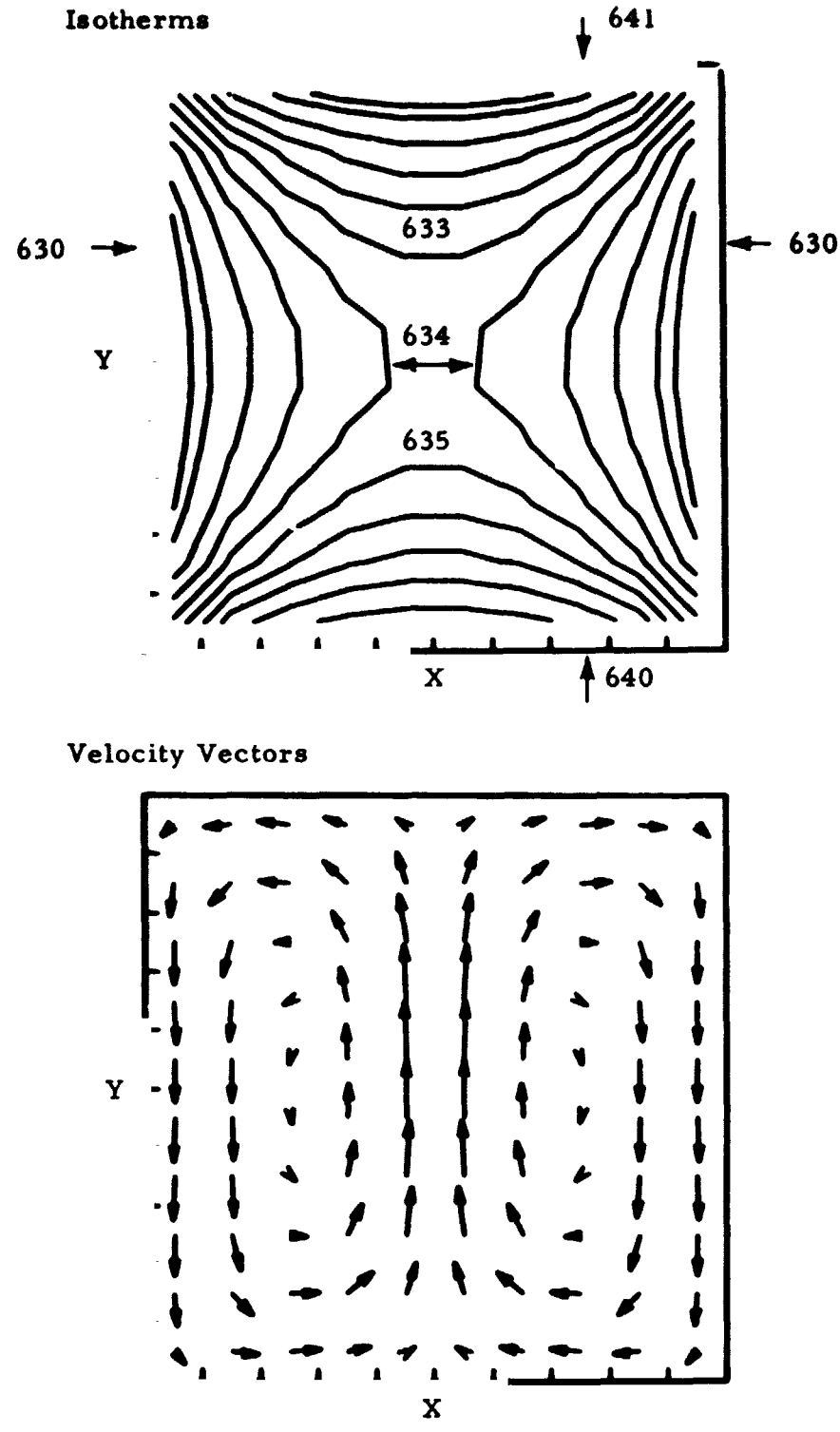

Fig. 16 - Isotherms and Velocity Profiles at t = 100 sec for *Al* Cu Case 12 (Thermal Convection); Max. Velocity = $7.6 \cdot 10^{-4}$ cm/sec; Isotherms in Degrees Celsius

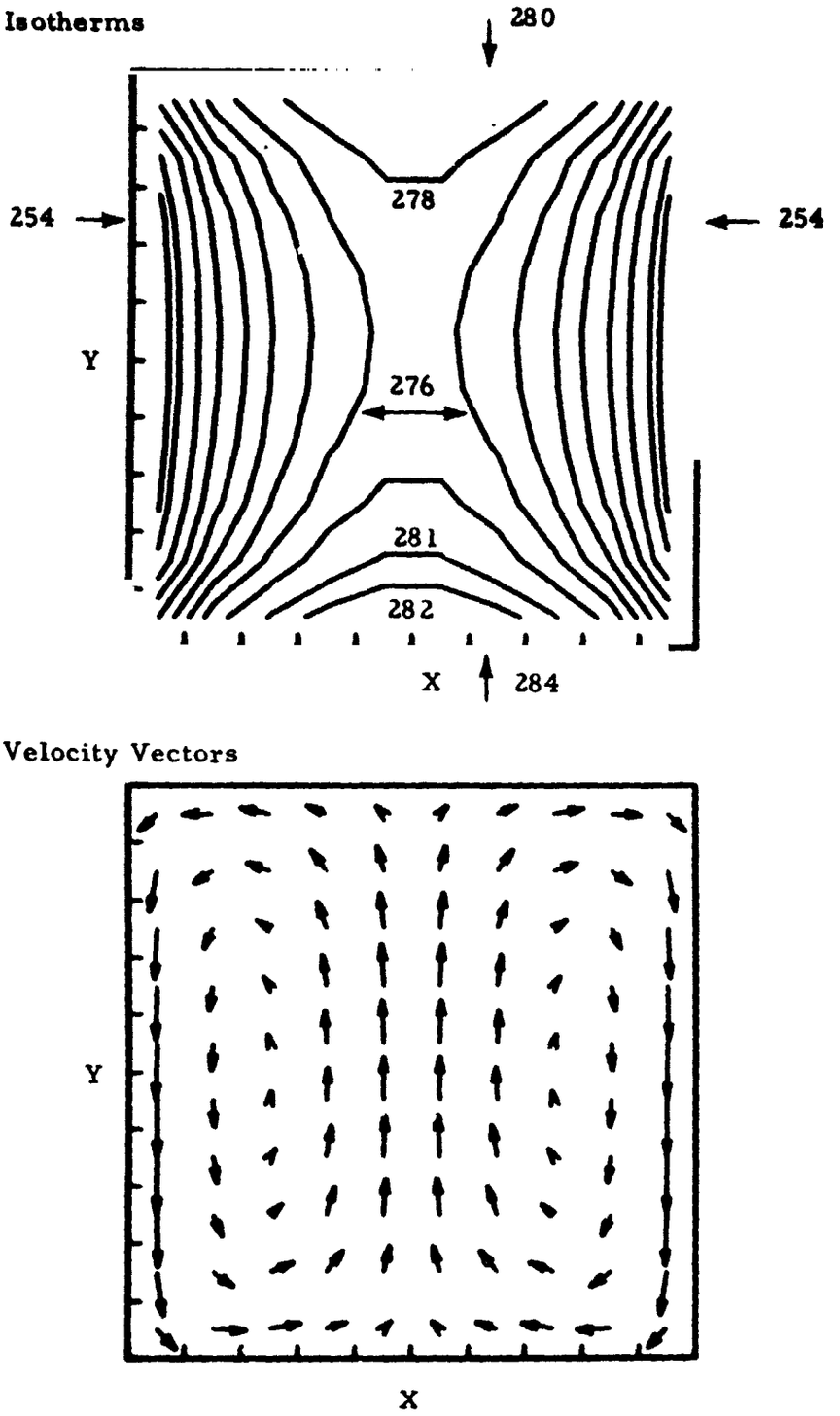

Fig. 17 - Isotherms and Velocity Profiles at t = 40 sec for SnBi Case 29 (Thermal Convection); $V_{max} = 2.5 \cdot 10^{-3}$ cm/sec; Isotherms in Degrees Celsius

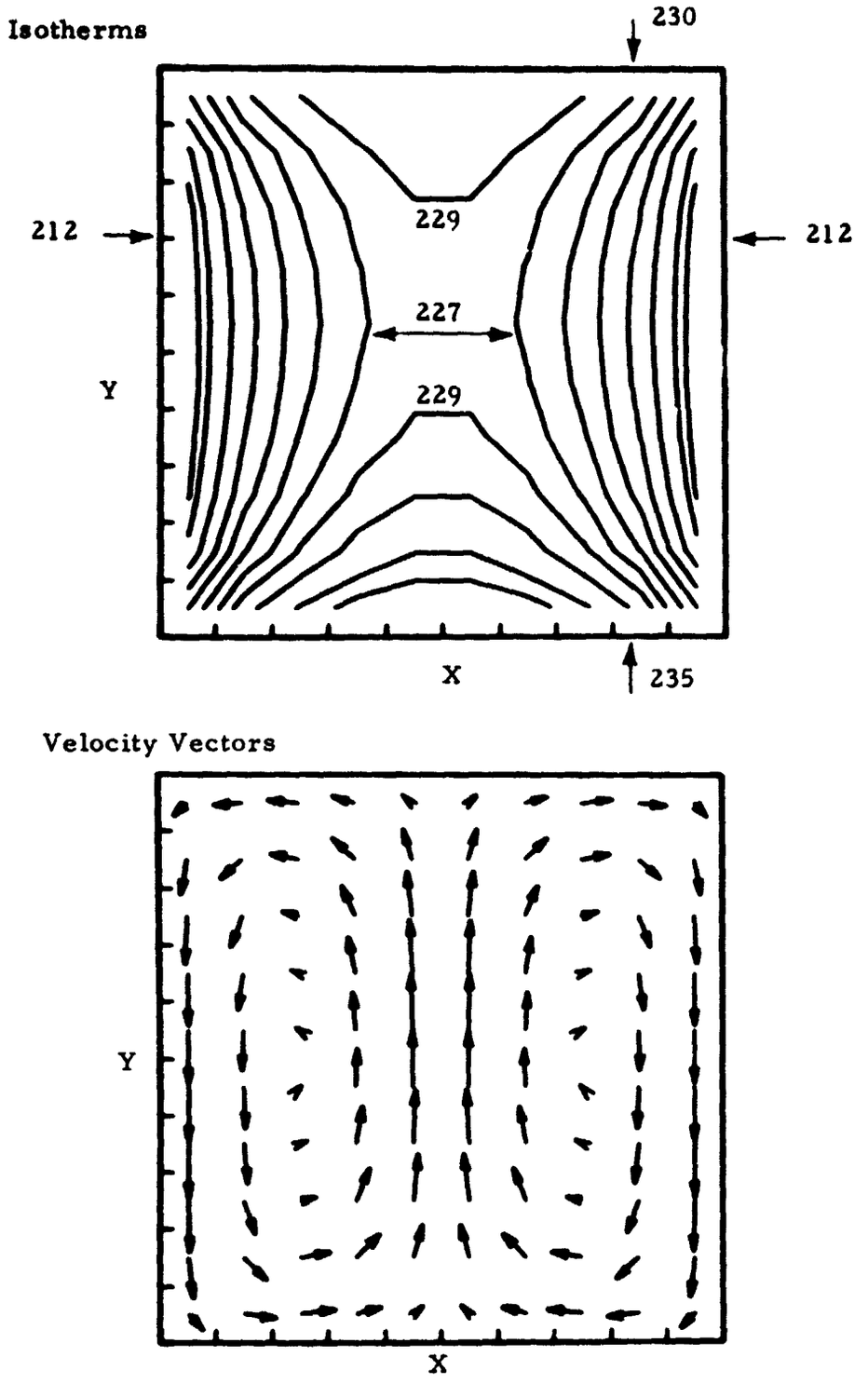

Fig. 18 - Isotherms and Velocity Profiles at t = 100 sec for SnBi Case 29 (Thermal Convection); $V_{max} = 3.9 \cdot 10^{-3}$ cm/sec; Isotherms in Degrees Celsius

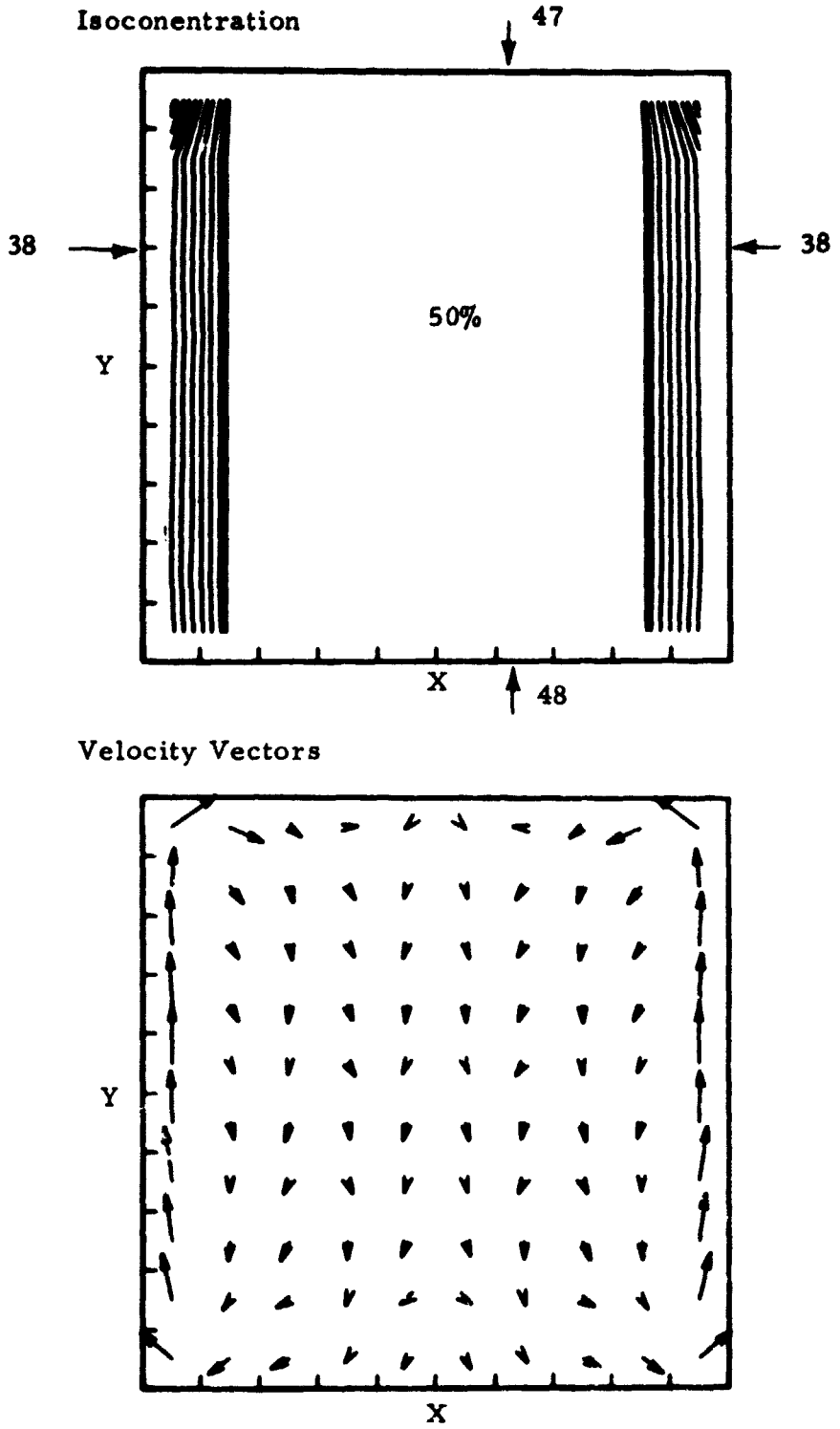

Fig. 19 - Isoconcentration and Velocity Profiles at t = 80 sec for SnPb Case 20 (Solutal Convection); $V_{max} = 2.6\ 10^{-5}$ cm/sec; Isoconcentrations in Wt. % Lead

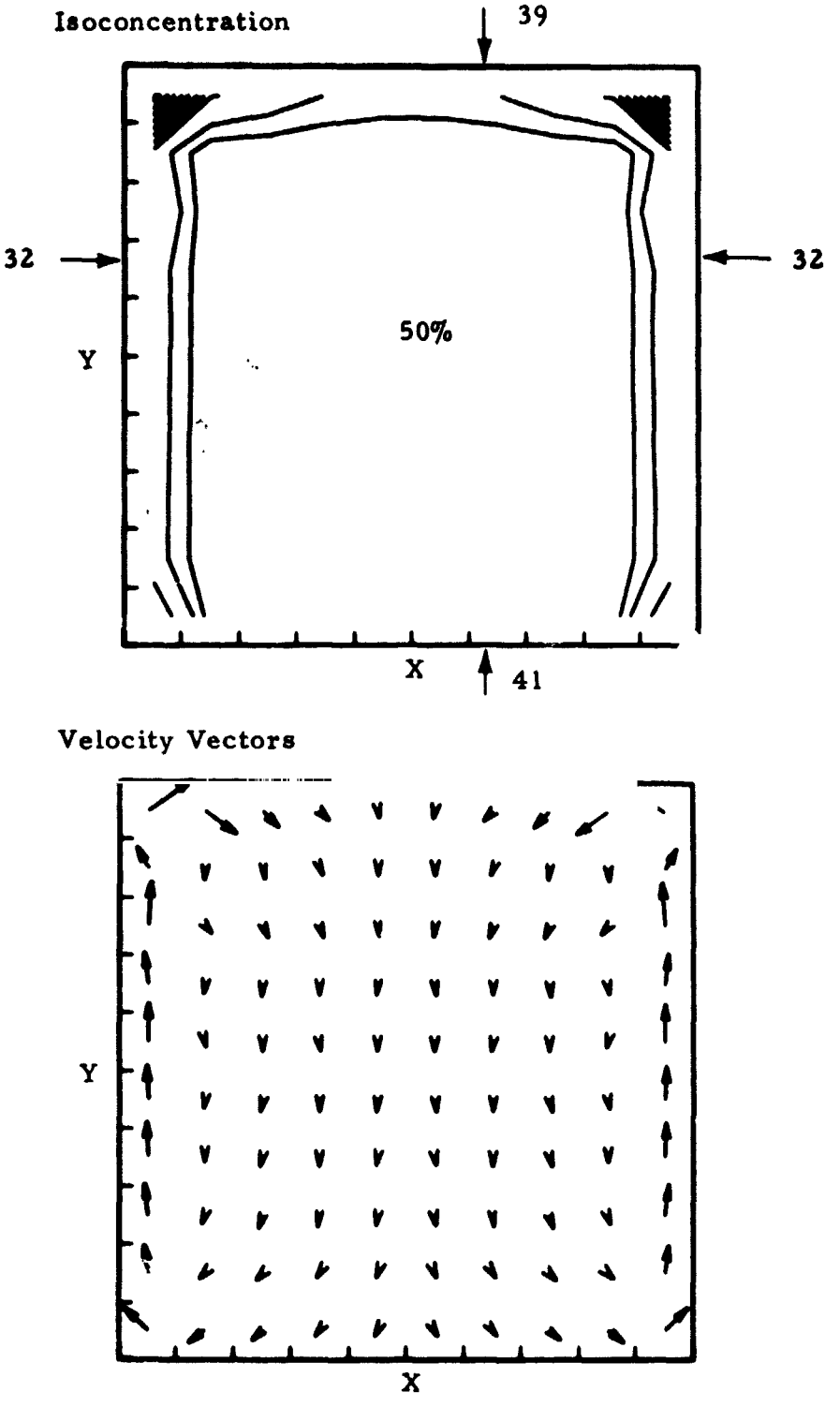

Fig. 20 - Isoconcentration and Velocity Profiles at t = 120 sec for SnPb Case 20 (Solutal Convection); $V_{max} = 3.5 \cdot 10^{-4}$ cm/sec; Isoconcentrations in Wt. % Lead

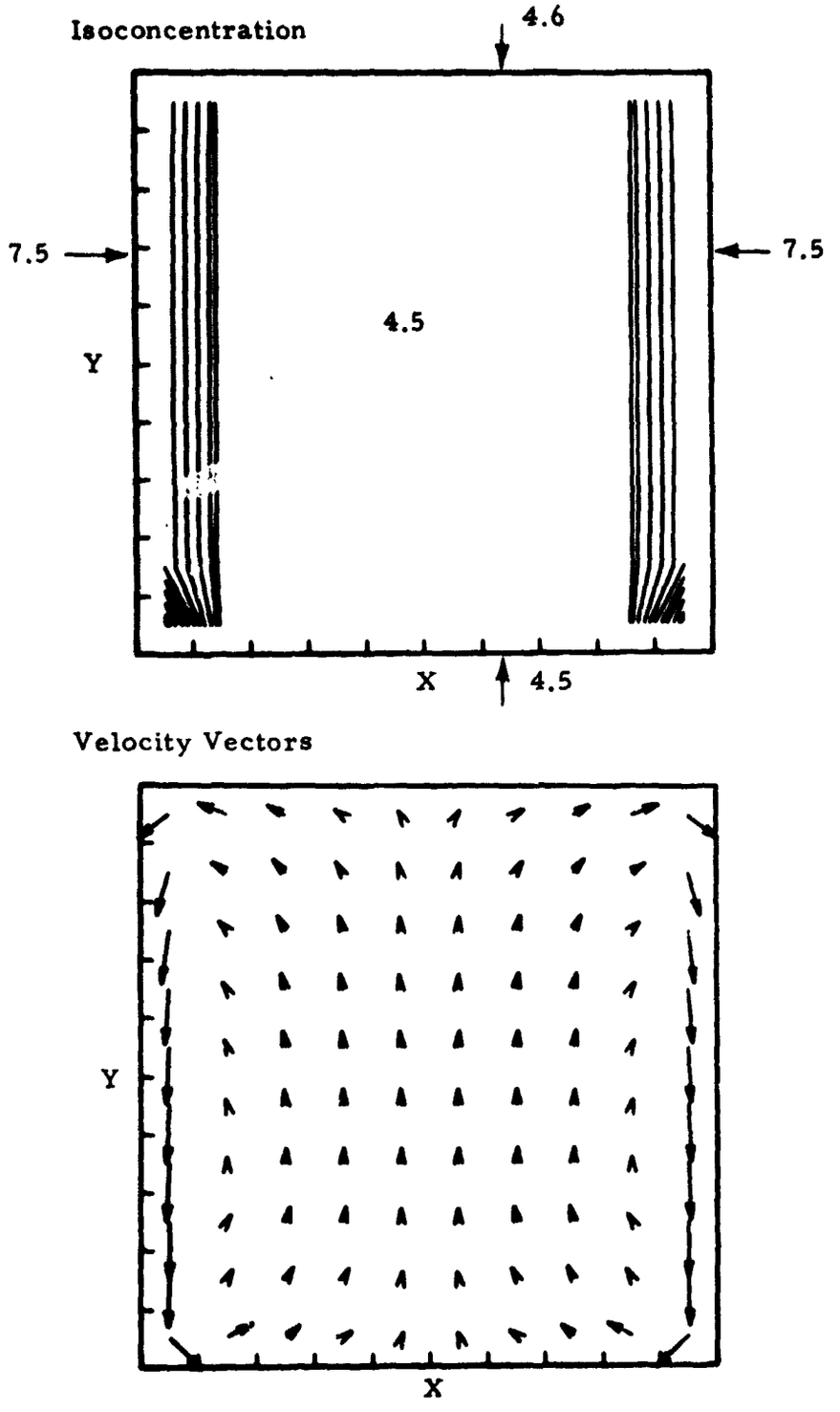

Fig. 21 - Isoconcentration and Velocity Profiles at t = 40 sec for Al Cu Case 12 (Solutal Convection); $V_{max} = 3.3 \cdot 10^{-4}$ cm/sec; Isoconcentrations in Wt. % Copper

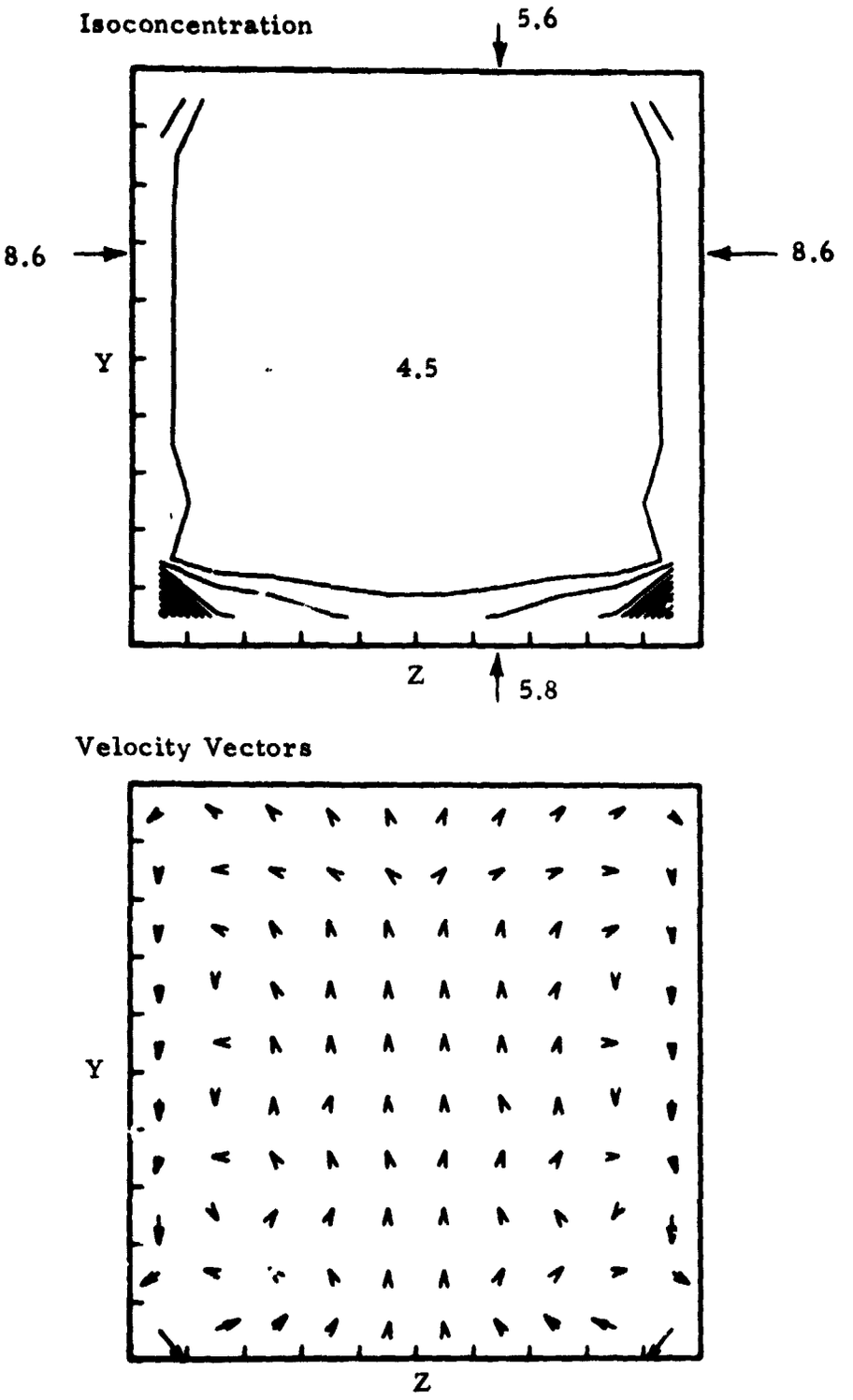

Fig. 22 - Isoconcentration and Velocity Profiles at t = 100 sec for Al Cu Case 12 (Solutal Convection); $V_{max} = 10^{-2}$ cm/sec; Isoconcentrations in Wt. % Copper

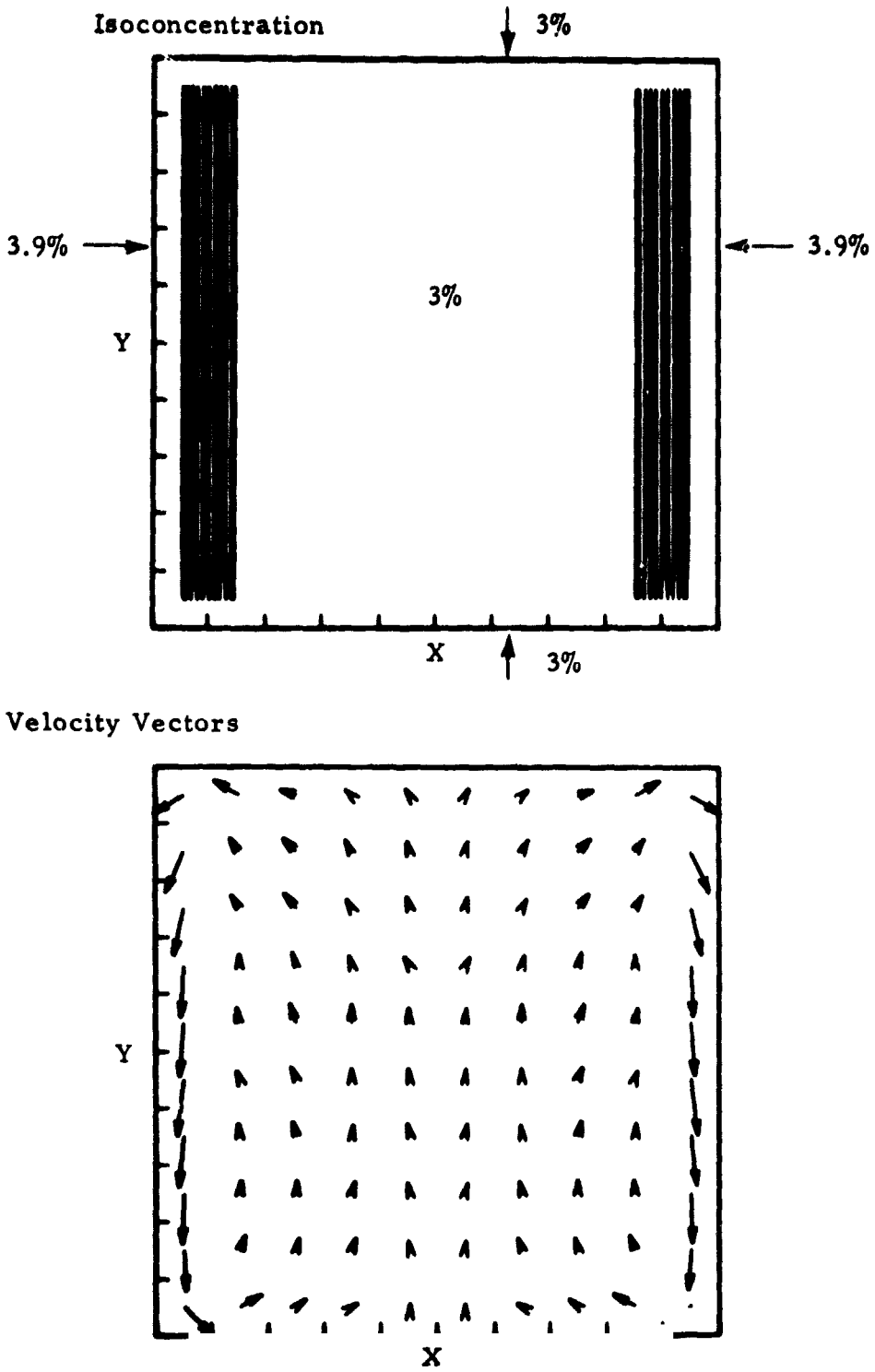

Fig. 23 - Isoconcentration and Velocity Profiles at t = 40 sec for SnBi Case 29 (Solutal Convection); $V_{max} = 1.3 \cdot 10^{-5}$ cm/sec; Isoconcentrations in Wt. % Bismuth

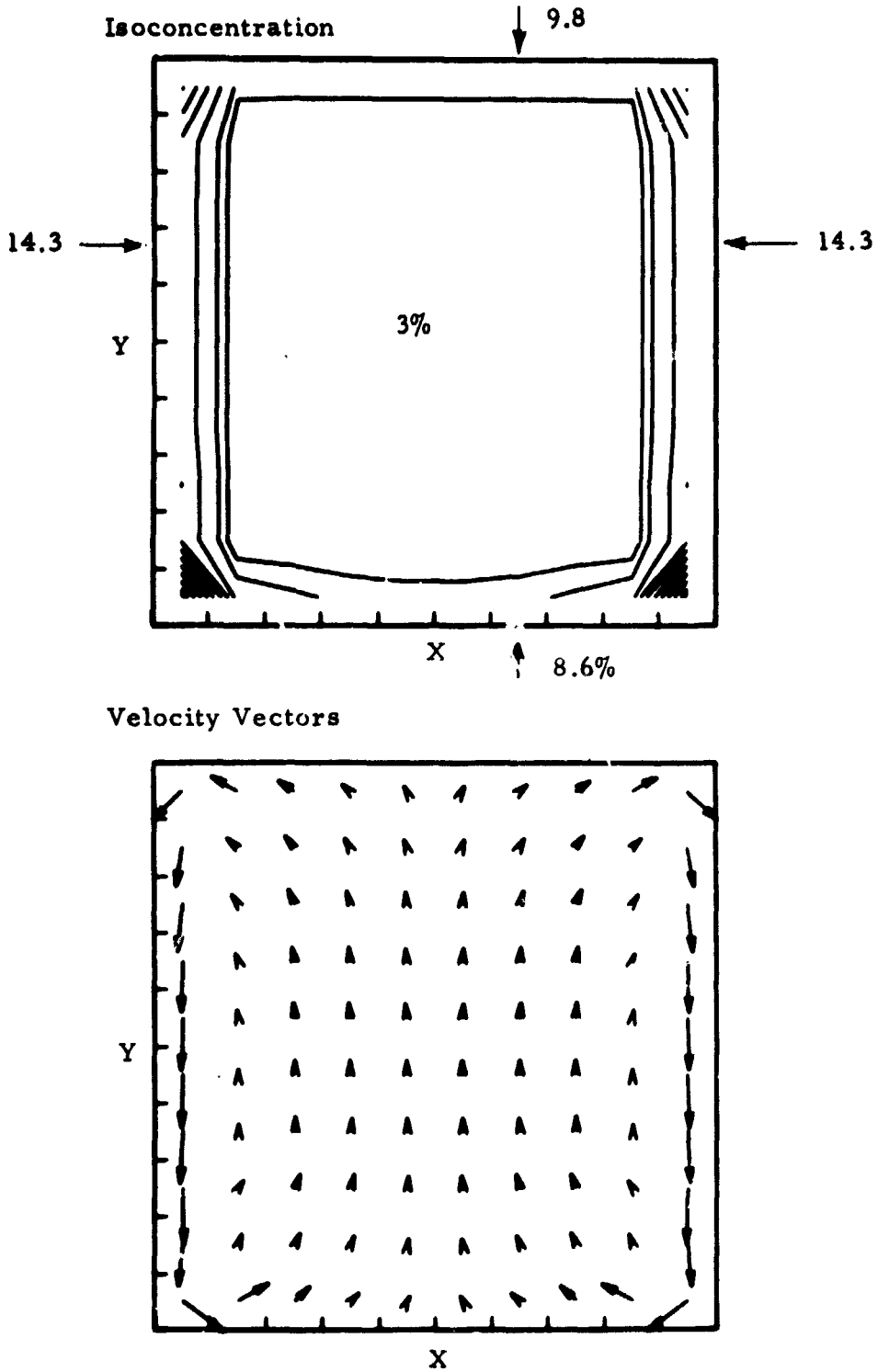

Fig. 24 - Isoconcentration and Velocity Profiles at t = 100 sec for SnBi Case 29 (Solutal Convection); $V_{max} = 1.9 \cdot 10^{-3}$ cm/sec; Isoconcentrations in Wt.% Bismuth

FLUID FLOWS GENERATED BY SPIN-UP AND DECAY TIMES

During the launch phase of a SPAR rocket flight, various accelerations occur. These are summarized as follows:

Stabilizing spin around longitudinal axis	240 rpm
Lateral accelerations due to aerodynamic forces (g-jitter)	$\pm$5 g, 0-4 Hz
Maximum g due to rocket acceleration	16 g

After about one minute after ignition, a "yo-yo" despin mechanism is deployed and the spin is brought down to about 0.2 deg/sec. Aerodynamic forces also become unimportant. Thus, the gravity environment becomes about 10^{-4} g at all points some 75 to 80 sec after ignition.

In the 76-36 experiment molten metal at its soak temperature will be sent up and will experience two periods of rotational acceleration — a spin-up and a spin-down — in rapid order before entering the low-g period. The question of what fluid motion is generated by the spin-up and how long it takes to decay after spin-down thus becomes of crucial importance. It may be mentioned that thrust acceleration and g-jitter induced flow should be insignificant because the melts will be essentially isothermal, homogeneous fluids.

The transient type of motion generated when a fluid filled cylinder is suddenly spun up is shown in Fig. 25. In Fig. 25 it should be kept in mind that the fluid sidewall layers are rotating while the center core remains irrotational for some time. A condition is finally reached where the entire body of fluid rotates as a unit. In the present simple analysis, it will be assumed that spin-up is complete in the liquid by the time the low-g phase of the flight is entered.

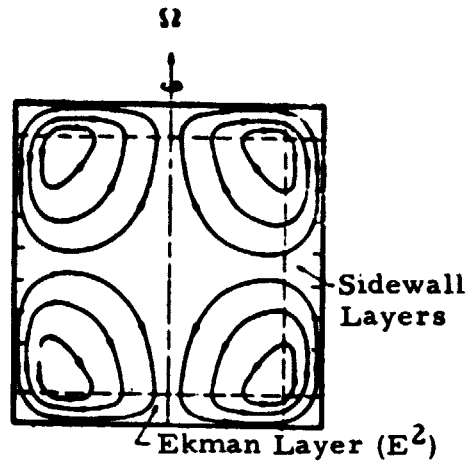

Fig. 25 - Schematic Drawing of Boundary Layers (Dashed) and Meridional Circulation Pattern Solid) for the Spin-Up of a Homogeneous Fluid in a Circular Cylinder (Ref. 9)

A prior treatment of spin-down times (Ref. 7) indicates that appropriate spin-down times can be calculated according to one of two analytical treatments in the literature, i.e.,

McLeod's analysis (Ref. 8) if $E^{1/4}\ L/2R \approx 1$
Benton's analysis (Ref. 9) if $E^{1/4}\ L/2R \ll 1$

where E is the Ekman number ($= \nu/\Omega\ L^2$), ν is the kinematic viscosity, Ω is the angular spin velocity, and L is the cylinder length, and R is the cylinder radius.

The cell of the 76-36 experiment is a thin rectangle which could be placed in one of two positions with respect to spin axis of the rocket, i.e., Fig. 26.

Values of $E^{1/4}\ L/2R$ can thus be calculated for three cases, i.e., Table 7.

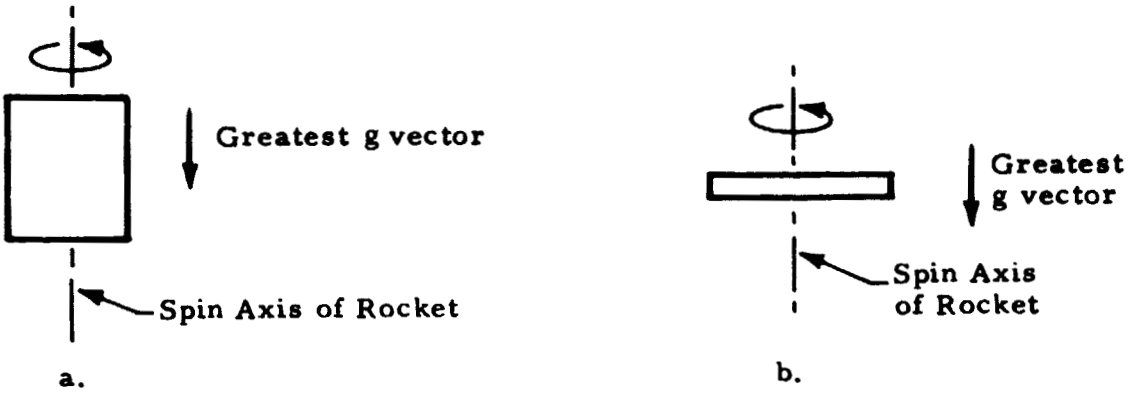

Fig. 26 - Two Possible Positions of 76-36 Cell with Respect to Rocket Spin Axis

Table 7

APPLICABLE THEORETICAL TREATMENTS FOR VARIOUS CASES

L	6.1 cm	6.1 cm	0.95 cm
R	0.475 cm (Effective Radius)	2.55 cm	2.55 cm
$E^{1/4}$ L/2R	0.62	0.057	0.022
Applicable Treatment	McLeod	Benton	Benton

The values given in Table 8 show the values of spin-down times for various cases and various treatments assuming a spin-down from about 240 to 1 rpm. A representative ν value of 5×10^{-3} cm^2/sec was used in the calculations.

Table 8

THEORETICAL SPIN-DOWN TIMES

Case	Theory	Cyl. Radius, R (cm)	Cyl. Length, L (cm)	Time (sec)
1	McLeod	0.475	Not Relevant	25.0
2	McLeod	2.55	Not Relevant	80.5
3	Benton	2.55	6.1	52.5
4	Benton	2.55	0.95	8.1

The values shown in Table 8 indicate that the shortest spin-down times occur in either Case (b), Fig. 26, or Case (a) if the assumption of an effective radius of 0.475 cm is valid, as it probably is.

Further information on spin-down times was obtained from Dr. L. L. Lacy of NASA-MSFC. Dr. Lacy in the past performed a number of rotation experiments with different fluids (including mercury) and containers. He found he could correlate his results by the following simple formula

$$T = \beta d^2/\nu$$

where T is the damping time (for the velocity to reach 5×10^{-3} cm/sec), β is a constant and equal to 0.102 for an end velocity 5×10^{-3} cm/sec, d is the cylinder diameter, and ν is the kinematic viscosity. Damping times calculated by Dr. Lacy's formula are as follows:

Diameter, d (cm)	Time, T (sec)
0.95 (Effective)	18.4
5.10	530.6

These results would indicate that Case (b), Fig. 26, would be undesirable.

Dr. Lacy performed one experiment in which a rectangular cell filled with water was spun slightly off axis, i.e., Fig. 27. It can be seen that the decay times are fairly short. Dr. Lacy also found that wetting and non-wetting conditions made a difference in the damping times (Table 9).

The conflicting results of theory and experiment is not apparent at present, but the length-to-diameter ratio (aspect ratio) is undoubtedly the crucial factor. Dr. Lacy's results are probably more applicable to tall, fat containers than to short, thin containers. In light of Dr. Lacy's experimental results on off-center placement and available theory, an orientation such as shown in Fig. 28 appears advisable. Also, as long a damping period as possible should be utilized, with 2 min as the absolute minimum.

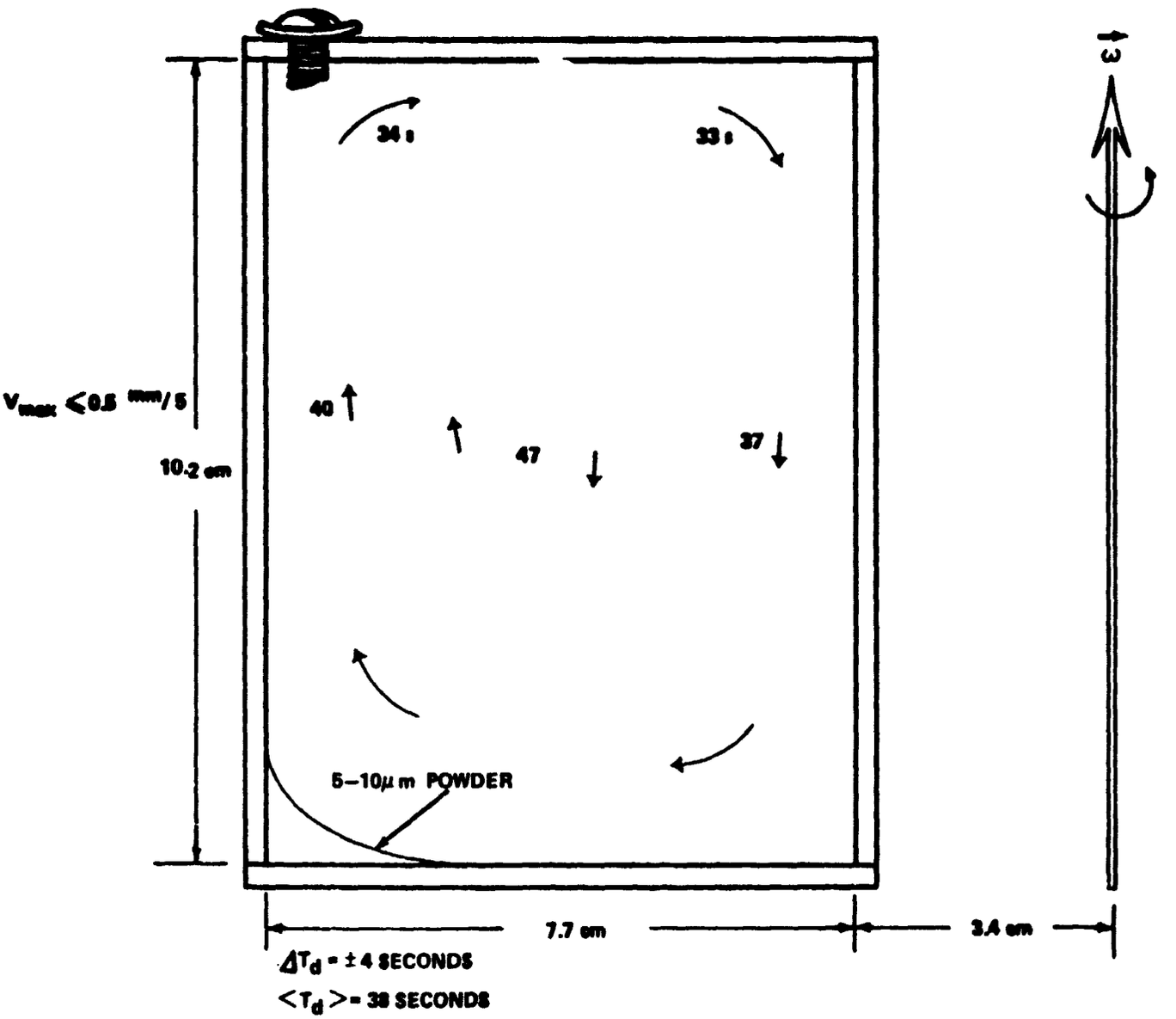

Fig. 27 - Vortex Motion and Decay Time for Rectangular Container of Water for SPA Rocket Experiment (Thickness: 1.3 cm) (Courtesy of Dr. L. L. Lacy, MSFC)

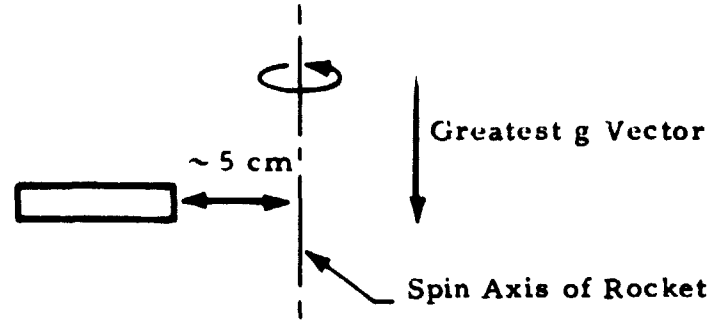

Fig. 28 - Recommended Orientation of Experiment Cell with Respect to Rocket Spin Axis

Table 9

TOTAL DECAY TIME AS A FUNCTION OF VARIOUS PARAMETERS
(Courtesy of Dr. L. L. Lacy, MSFC)

Fluid	Container Material	Diameter and Length (cm)	Wetting or Nonwetting	Decay Time (sec)	Conditions
Water	Plastic	2.15 5.6	W	36 ± 2	Center Vial
	Plastic	2.15 5.6	W	31 ± 3	Vial 2" Off Center of Rotation
	Plastic	2.15 5.6	W	2	Vial with Vertical Baffle
	Plastic	1.15	W	10 ± 1	Vial 2" Off Center
	Glass	1.69 5.0	W	20 ± 1	Center Vial
	Glass	1.69 5.0	N	18.6 ± 0.7	Same as Above Except Coated with Krylon
	Glass	1.69 5.0	N	18.3 ± 1.5	Coated with Dow Corning 200 Fluid
	Glass	1.69 5.0	N	17.5 ± 1.5	Coated with RAM Mold Release 225
	Glass	2.38 7.4	W	46.8 ± 0.9	Center Vial
Carbon Tetra-Chloride	Glass	1.69 4.2	W	30.3 ± 0.9	Center Vial
Cyclo-hexanol	Glass	1.69	W	< 1	Center Vial
Mercury	Plastic	2.15 2.8	N	186 ± 10	Center Vial
	Plastic	1.69 2.95	N	95 ± 5	Center Vial

REFERENCES

1. Johnston, M. H., and C. S. Griner, "The Direct Observation of Solidification as a Function of Gravity Level," Met. Trans. A, Vol. 8A, 1977, pp. 77-82.
2. Grodzka, P. G., J. E. Pond, and L. W. Spradley, "Thermal and Convection Analyses of the Dendrite Remelting Rocket Experiment; Experiment 74-21 in the Space Processing Rocket Program," Final Report, Contract NAS8-31800, LMSC-HREC TR D496847, Lockheed Missiles & Space Company, Huntsville, Ala., 31 May 1976.
3. Flemings, M. C., Solidification Processing, McGraw-Hill, New York, 1974.
4. Coulthard, J. O., and R. Elliot, "Cellular/Cellular-Dendritic Transition in Single-Phase Alloys," The Solidification of Metals, Conference sponsored by The Iron and Steel Institute and others, Brighton, England, 4-7 December 1967, published by the Iron and Steel Institute.
5. Walton, D., W. A. Tiller, J. W. Rutter and W. C. Winegard, "Instability of a Smooth Solid-Liquid Interface During Solidification," J. Metals, Trans. AIME, September 1955, pp. 1023-1025.
6. Holmes, E. L., J. W. Rutter and W. C. Winegard, "Growth Conditions for Stability of a Cellular Solid-Liquid Interface," Can. J. Phys., Vol. 37, 1957, pp. 1223-1227.
7. Unpublished analysis by Dr. S. V. Bourgeois of Lockheed-Huntsville.
8. McLeod, A. R., "The Unsteady Motion Produced in a Uniformly Rotating Cylinder of Water by a Sudden Change in Angular Velocity of the Boundary," Phil. Mag., Vol. 44, 6th Series, 1922, pp. 1-14.
9. Benton, E. R., and A. Clark, Jr., "Spin-Up," Annual Rev. of Fluid Mechanics, Vol. 6, 1974, pp. 257-280.